

Parameter-Efficient Fine-Tuning in Spectral Domain for Point Cloud Learning

Dingkang Liang, Tianrui Feng, Xin Zhou, Yumeng Zhang, Zhikang Zou, Xiang Bai

Abstract—Recently, leveraging pre-training techniques to enhance point cloud models has become a hot research topic. However, existing approaches typically require full fine-tuning of pre-trained models to achieve satisfied performance on downstream tasks, accompanying storage-intensive and computationally demanding. To address this issue, we propose a novel Parameter-Efficient Fine-Tuning (PEFT) method for point cloud, called **PointGST** (**P**oint cloud **G**raph **S**pectral **T**uning). PointGST freezes the pre-trained model and introduces a lightweight, trainable Point Cloud Spectral Adapter (PCSA) to fine-tune parameters in the spectral domain. The core idea is built on two observations: 1) The inner tokens from frozen models might present confusion in the spatial domain; 2) Task-specific intrinsic information is important for transferring the general knowledge to the downstream task. Specifically, PointGST transfers the point tokens from the spatial domain to the spectral domain, effectively de-correlating confusion among tokens via using orthogonal components for separating. Moreover, the generated spectral basis involves intrinsic information about the downstream point clouds, enabling more targeted tuning. As a result, PointGST facilitates the efficient transfer of general knowledge to downstream tasks while significantly reducing training costs. Extensive experiments on challenging point cloud datasets across various tasks demonstrate that PointGST not only outperforms its fully fine-tuning counterpart but also significantly reduces trainable parameters, making it a promising solution for efficient point cloud learning. More importantly, it improves upon a solid baseline by +2.28%, 1.16%, and 2.78%, resulting in 99.48%, 97.76%, and 96.18% on the ScanObjNN OBJ_BG, OBJ_OBLY, and PB_T50_RS datasets, respectively. This advancement establishes a new state-of-the-art, using only 0.67% of the trainable parameters. The code will be made available at <https://github.com/jerryfeng2003/PointGST>.

Index Terms—Point Cloud, Efficient Tuning, Spectral.

1 INTRODUCTION

POINT cloud learning is a fundamental and highly practical task within the computer vision community, drawing significant attention due to its extensive applications such as autonomous driving [13], [31], 3D reconstruction [45], [80], and embodied intelligence [82], among others. Different from images, point clouds are inherently sparse, unordered, and irregular, posing unique challenges to effective analysis.

Nowadays, exploring pre-training techniques to boost the models has become a hot research topic in both natural language processing [9] and computer vision [21], and has been successfully transferred to the point cloud domain [36], [47], [75], [85]. For example, representative works like PointBERT [85] and Point-MAE [47] introduce the Mask Point Modeling task for point cloud, and the subsequent studies [4], [11], [36], [93] propose effective customized pre-training tasks. After pre-training, these methods adopt the classical fully fine-training (FFT) strategy, where all models' parameters are fine-tuned, leading to notable performance improvements and faster convergence compared to training from scratch. However, the FFT incurs significant computational costs, particularly in terms of GPU memory and storage, since fine-tuning the entire pre-trained models involves updating a large number of parameters. With the scaling of

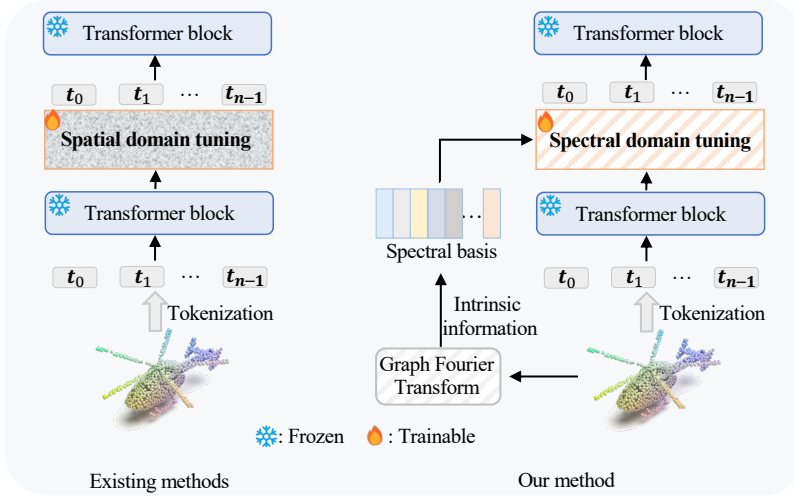
models¹ or increasing needs to fine-tuning enormous new datasets, the demand for storing fine-tuned checkpoints grows, resulting in heightened storage and memory consumption.

The community is well aware of this issue, and to mitigate this challenge, research efforts [15], [64], [88], [99] have been put on looking for a promising fine-tuning strategy, i.e., Parameter-Efficient Fine-Tuning (PEFT). Their common idea is to freeze the pre-trained models and simply insert extra learnable parameters in the models. The pioneers are IDPT [88] and DAPT [99], taking an important step toward efficient tuning on point cloud tasks. Specifically, IDPT [88] proposes an instance-aware dynamic prompt tuning to generate a universal prompt for the point cloud data. DAPT [99] generates a dynamic scale for each point token, considering the token significance to the downstream task.

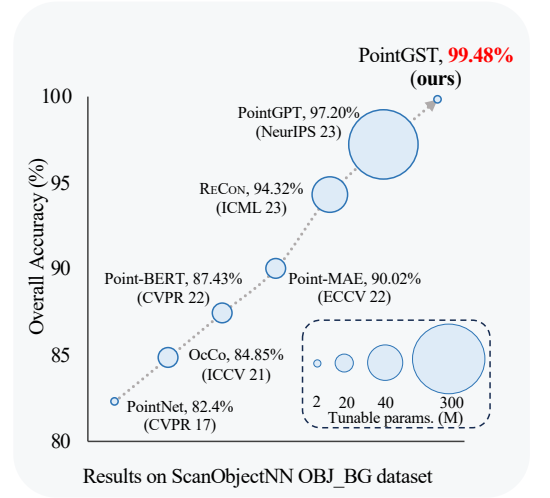
While the above methods have demonstrated efficiency in terms of training and storage, they still fail to achieve satisfactory performance across various pre-trained models. We attribute this to two-fold: **First**, essentially, these methods are fine-tuned in the spatial domain (Fig. 1(a)). In the PEFT setting, pre-trained tasks are designed to learn general representations of point clouds and lack downstream tasks prior. This leads to the inner tokens (features) from frozen pre-trained models that struggle to distinguish the fine-grained structures of the point cloud, where such tokens are referred to as inner confused tokens. Current point cloud PEFT methods fine-tune in the spatial domain by merging

- Dingkang Liang, Tianrui Feng, Xin Zhou, and Xiang Bai are with Huazhong University of Science and Technology. (dkliang, tianruifeng, xzhou03, xbai)@hust.edu.cn
- Yumeng Zhang and Zhikang Zou are with Baidu Inc., China.
- Dingkang Liang, Tianrui Feng, and Xin Zhou make equal contributions. The corresponding author is Xiang Bai (xbai@hust.edu.cn).

¹Pre-trained point cloud model parameters increased 30× in three years, from 22.1M in ECCV 2022 [47] to 657.2M in ECCV 2024 [51].



(a) The comparison between existing PEFT methods (left) and our method (right)



(b) The comparisons in terms of performance and trainable parameters

Fig. 1: (a) The comparison of existing PEFT methods [88], [99] and our method. Instead of spatial tuning, we transform the point cloud to the spectral domain to mitigate the confusion among tokens and bring the intrinsic information of the downstream point clouds for targeted tuning. (b) The proposed PointGST outperforms all previous point cloud analysis methods while using extremely few trainable parameters. We even achieve a remarkable accuracy of 99.48% on the popular ScanObjectNN OBJ_BG dataset, pushing the performance on this dataset to surpass 99% for the first time.

inner confused tokens with newly introduced learnable modules for downstream task adaptation, making it challenging to de-correlate the inherent confusion of the tokens. **Second**, intrinsic structures (e.g., task-specific geometry and relationship of points) of the downstream point clouds are essential for comprehensive analysis [17], [80]. The fixed pre-trained models lack the ability to update their parameters to learn the intrinsic information, relying solely on the representations captured during pre-training. Existing point cloud PEFT methods mainly utilize the encoded features from the frozen models to generate prompts or feed into adapters, which do not explicitly introduce the intrinsic information of the downstream point clouds.

Considering the above issues, we shift our focus to a new perspective: spectral domain fine-tuning. Spectral representations offer significant distinctness over spatial domain representations. Specifically, compared to the spatial domain, features in the spectral domain can be easily de-correlated [57], [90], due to the ability of spectral representations to disentangle complex spatial relationships into distinct frequency components. This decorrelation mitigates the confusion among tokens by using orthogonal components (spectral basis) to separate them. Additionally, the spectral basis obtained by the original point cloud offers direct intrinsic information about the downstream tasks to better guide the fine-tuning process. However, effectively and efficiently fine-tuning the parameters in the spectral domain is not a trivial problem, where two crucial concerns need to be considered: 1) what spectral transform to use, and 2) how to inject the intrinsic information into the fixed pre-trained model by using this transform. An ideal transform for point clouds should be easy to construct, preserve intrinsic information, and adapt to the irregular structure of point cloud data. We find that the Graph Fourier Transform (GFT)

stands out as particularly suitable. A properly constructed graph can provide a natural representation of the irregular point clouds that are adaptive to their structure, and the graph spectral domain can explicitly reveal geometric structures, from basic shapes to fine details, within a compressed space [25].

In this paper, we explore the potential of fine-tuning parameters in the spectral domain. Our approach, illustrated in Fig. 1(a), introduces a novel PEFT method that optimizes a frozen pre-trained point cloud model through Graph Spectral Tuning, which we refer to as **PointGST**. Specifically, we first construct a series of multi-scale point cloud graphs that enable the calculation of global and local spectral basis, which will bring the intrinsic information like the geometry of the original point cloud. Then, we propose a lightweight Point Cloud Spectral Adapter (PCSA) to transform the point tokens (serving as graph signal) from the spatial domain to the spectral domain using the spectral basis. Based on the spectral point tokens, our PCSA adopts an effortless shared linear layer to adapt the global and local spectral tokens to meet the downstream tasks. In the spectral domain, adjusting parameters actually modifies the “energy” of each graph frequency for the graph signal, improving the decorrelation of the inner confused tokens when transforming back to the spatial domain. Besides, the information of the generated spectral basis is inherently aware of the unique characteristics of the downstream point clouds, enabling targeted fine-tuning.

Extensive experiments conducted on challenging point cloud datasets across various tasks and data settings demonstrate the effectiveness of our PointGST. For example, when adopting the convincing Point-BERT [85] (resp., Point-MAE [40]) as the baseline, our approach archives notable performance improvement over fully fine-tuning

by 3.96%, 1.55%, 2.57%, and 0.7% (*resp.*, 1.72%, 1.90%, 0.11%, and 0.3%) on the ScanObjectNN OBJ_BG, OBJ_ONLY, PB_T50_RS and ModelNet40 datasets, while surprisingly only requires about 2.77% of the total learnable parameters. More importantly, our method even boosts the large-scale pre-trained models PointGPT-L [4], only using 0.6% trainable parameters to achieve 99.48% accuracy on the ScanObjectNN OBJ_BG dataset, outperforming the SOTA method PointGPT-L [4] by 2.28%, establishing the new state-of-the-art. To the best of our knowledge, we are the first to push the performance on this dataset to surpass 99%. We also draw the intuitive trend of performance and trainable parameters in Fig. 1(b).

Our main contributions are summarized as follows: **1)** In this paper, we propose a novel Parameter-Efficient Fine-Tuning (PEFT) method for point cloud learning, named **PointGST**, which innovatively fine-tunes parameters from a fresh perspective, i.e., spectral domain. **2)** PointGST introduces the Point Cloud Spectral Adapter (PCSA) for frozen pre-trained backbones, transferring the inner confused tokens from the spatial domain into the spectral domain. It effectively mitigates the confusion among tokens and brings intrinsic information from downstream point clouds to meet the requirement of fine-tuned tasks. **3)** Extensive experiments across various datasets demonstrate that our proposed method outperforms all current point cloud-customized PEFT approaches. Remarkably, we achieve state-of-the-art performance on six challenging point cloud datasets while only using about 0.6% trainable parameters, serving as a promising option for fine-tuning the point cloud data.

2 RELATED WORKS

2.1 Point Cloud Learning

Constructing structural representations for the point cloud has become a core topic in the computer vision community. To address the irregularity and sparsity of point clouds, the pioneering PointNet [48] adopts shared MLP layers to extract point features independently. The subsequent works further integrate local and global information [37], [49], [52], [56], [61], [72], self-attention mechanisms [19], [77], [78], [96], and various regularization techniques [75], [92], [94], prompting the field.

More recently, self-supervised pre-training methods [16], [36], [50], [81], [85], [98], have gained significant attention in the domain for their remarkable transfer capabilities by learning latent representations from unlabeled data and then fine-tuning on various downstream tasks. Point cloud pre-training approaches can be categorized into contrast-based [1], [6], [81] and reconstruct-based [4], [11], [47], [51], [85], [93] paradigms. In the contrast-based paradigm, PointContrast [81] and CrossPoint [1] extract latent information from different views of the point cloud. Conversely, reconstruction-based methods involve randomly masking point clouds and then using autoencoders to reconstruct the original input. Among them, Point-BERT [85] learns by comparing masked encodings with outputs from a dVAE-based point cloud tokenizer. Point-MAE [47] and Point-M2AE [93] reconstructs original point clouds via an autoencoder. Following this, PointGPT [4] leverages an extractor-

generator-based transformer as a GPT-style approach. To tackle data scarcity in 3D representation learning, interest in using cross-modal data for point cloud analysis is growing. For instance, ACT [11] trains 3D representation models using cross-modal pre-trained models as teachers, and RECON [50], [51] unifies reconstruction and cross-modal contrast modeling further.

Generally, these pre-training approaches typically transfer to the downstream 3D point cloud analysis tasks by fully fine-tuning the pre-trained models. However, as model parameters rapidly increase with scaling up [4], [51], fully fine-tuning incurs high tuning and storage costs and may dilute the pre-training knowledge. This paper seeks to reduce training costs through efficient transfer learning algorithms.

2.2 Parameter-Efficient Fine-Tuning

Parameter-Efficient Fine-Tuning (PEFT) aims to adopt a trainable module with a few parameters for fine-tuning. It has become a hot research topic in both the NLP [7], [10], [58], [62], [91] and computer vision [26], [35], [67], [86] communities. The mainstream PEFT methods can be roughly categorized into Adapter-based and Prompt-based.

Specifically, the Adapter-based [7], [23], [24], [33], [62] methods usually insert a trainable module between frozen modules to adjust the pre-trained models. Particularly, Adaptformer [7] adds the adapter [23] in the FFN for the visual recognition tasks. The Prompt-based methods [26], [29], [34], [58] usually leverage the additional tokens (i.e., prompts) to the model input. For example, VPT [26], the first prompt-tuning method for vision tasks, prepends additional tunable tokens to the input or hidden layers of ViTs. Apart from paradigms mentioned above, some methods make new attempts, such as directly performing a linear transformation to modulate the features [35] or fine-tuning the bias term in each layer [86].

Recently, some works [14], [15], [32], [60], [63], [64], [88], [99] attempt to explore the PEFT in point cloud tasks. As the earliest method, IDPT [88] applies DGCNN [74] to extract dynamic prompts for different instances instead of the traditional static prompts. Point-PEFT [64] attempts to aggregate local point information during fine-tuning. DA [15] introduces a dynamic aggregation strategy to replace previous static aggregation like mean or max pooling for pre-trained point cloud models. Recently, DAPT [99] proposes an approach combining the dynamic scale adapters with internal prompts as an efficient way of point cloud transfer learning. Although these methods can effectively reduce training costs, they are difficult to achieve the desired performance consistently and generalize poorly. We argue it is attributed to the limitation of fine-tuning in the spatial domain and lack of introducing strong intrinsic information of downstream point cloud. In contrast, we try to fine-tune the parameters in the spectral domain, which effectively mitigates the confusion among tokens and brings intrinsic information about downstream point clouds.

2.3 Spectral Methods for Point Clouds

Methods that utilize spectral information to understand point clouds achieve notable advancements [5], [30], [43], [66]. For example, Wang et al. [71] combine spectral feature

learning with recursive clustering to overcome the isolated local feature aggregation. Zhang et al. [95] introduce tensor-based methods to estimate hypergraph spectrum components and frequency coefficients of point clouds in both ideal and noisy settings. GSDA [39] proposes the graph spectral domain attack, perturbing graph transform coefficients in the spectral domain. PointWavelet [76] designs graph wavelet transform to avoid the very time-consuming spectral decomposition. Ramasinghe et al. [54] propose a spectral-domain GAN that generates novel 3D shapes by using a spherical harmonics-based representation.

In this paper, we focus on the practical Parameter-efficient Fine-Tuning (PEFT) task, and propose a fresh PEFT method named PointGST for point cloud tasks, which efficiently fine-tunes the given pre-trained point cloud models in the spectral domain. The fundamental goals and techniques between our method and previous spectral-based point cloud methods are different.

3 PRELIMINARY

This section revisits the mainstream fine-tuning paradigms and introduces the concept of Graph Fourier Transform.

3.1 Fine-Tuning Paradigm

Fully Fine-Tuning (FFT) is the most commonly used fine-tuning paradigm. Given a downstream training set $\Gamma(x; y)$ (x is the input and y is the label), the FFT trains the network $\mathcal{F}(x; \theta)$ and obtains the updated weight θ^* , where θ is the trainable parameters of \mathcal{F} . Specifically, the FFT paradigm can be formulated as:

$$\theta^* = \arg \min_{\theta} \ell(\mathcal{F}(x; \theta), y), \quad (1)$$

where ℓ represents the loss function for downstream tasks. Notably, the FFT updates θ to θ^* , and θ^* retains the same shape as θ after fine-tuning. In general, FFT will bring notable training costs reflected in GPU memory and storage.

Parameter-Efficient Fine-Tuning (PEFT) provides a practical solution by adapting pre-trained models to downstream tasks in a more efficient manner. Existing PEFT methods focus on tuning only a small subset of parameters θ' . The optimized parameter θ'^* can be represented as:

$$\theta'^* = \arg \min_{\theta'} \ell(\mathcal{F}(x; \theta, \theta'), y), |\theta'| \ll |\theta|. \quad (2)$$

The magnitude of $|\theta'^*|$ equals $|\theta'|$ and is significantly smaller than the pre-trained θ . During fine-tuning, the pre-trained θ remains fixed while only θ' is update to θ'^* . Techniques for incorporating θ' include adding lightweight additional parameters and selecting a small subset of the pre-trained θ .

Adapter-like methods [7], [23], [84], adding lightweight extra parameters, are typical of the PEFT paradigm. Specifically, an Adapter-based approach usually includes a down-sampling layer W_d to reduce the feature dimension C to r , an activation function Φ , and an up-sampling layer W_u to recover the dimension. The low-rank dimension r ($r \ll C$) serves as a hyper-parameter for adapters. The formulation can be expressed as:

$$\hat{x} = \Phi(xW_d^\top)W_u^\top, \quad (3)$$

where $x \in \mathbb{R}^{n \times C}$ represents the input vectors from a pre-trained model. The output \hat{x} is added back to the original computation graph, with multiple Adapter structures comprising the new parameters θ' .

3.2 Graph Fourier Transform

Let us define a graph $\mathcal{G} = \{\mathcal{V}, \mathcal{E}, \mathcal{W}\}$, where \mathcal{G} is the set of vertices ($|\mathcal{G}| = n$), \mathcal{E} represents the edges, and \mathcal{W} is the adjacency matrix. In our context, a graph signal $z \in \mathbb{R}^{n \times c}$ assigns a vector ($z_i \in \mathbb{R}^{1 \times c}$) to each vertex, while the entry $w_{i,j}$ in \mathcal{W} indicates the weight of the edge between vertices i and j , reflecting their similarity. Then the Laplacian matrix is defined as $L = D - \mathcal{W}$ [59], where D is a diagonal matrix with each element $d_{i,i} = \sum_{j=0}^{n-1} w_{i,j}$ representing the degree of vertex i . For an undirected graph with non-negative weights, $L \in \mathbb{R}^{n \times n}$ is real, symmetric, and positive semi-definite [8]. This allows for the eigen-decomposition $L = U\Lambda U^\top$, where $U = [u_0, \dots, u_{n-1}]$ is an orthonormal matrix composed of eigenvectors u_i , and eigenvalues $\Lambda = \text{diag}(\lambda_0, \dots, \lambda_{n-1})$ are often interpreted as the graph frequencies.

Specifically, the eigenvectors above can be viewed as a set of spectral basis, allowing the Graph Fourier Transform (GFT) of the graph signal z to be expressed as:

$$\hat{z} = \text{GFT}(z) = U^\top z, \quad (4)$$

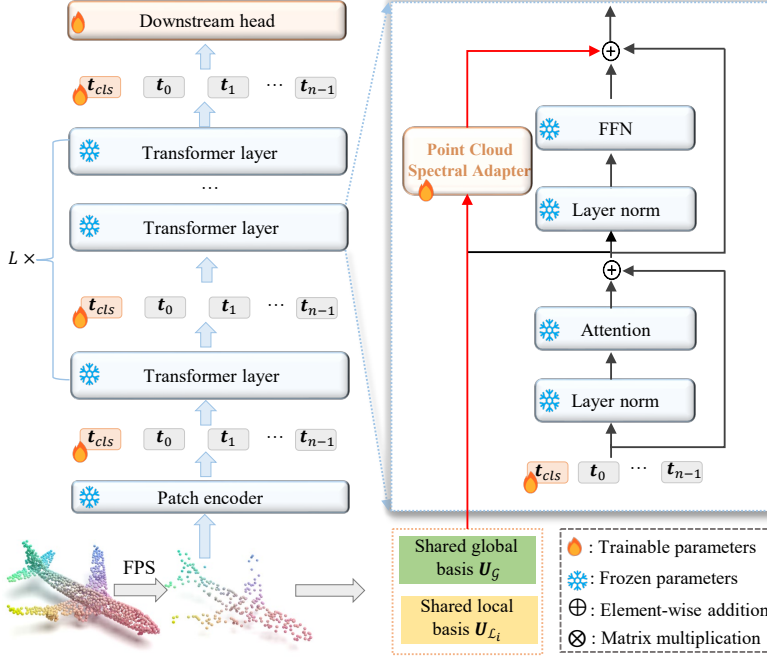
where $\hat{z} \in \mathbb{R}^{n \times c}$ represents the spectral coefficients for different graph frequencies, with the square of each column indicating the “energy” of the corresponding frequency. Similarly, the inverse Graph Fourier Transform (iGFT) is then defined as:

$$z = \text{iGFT}(\hat{z}) = U\hat{z}. \quad (5)$$

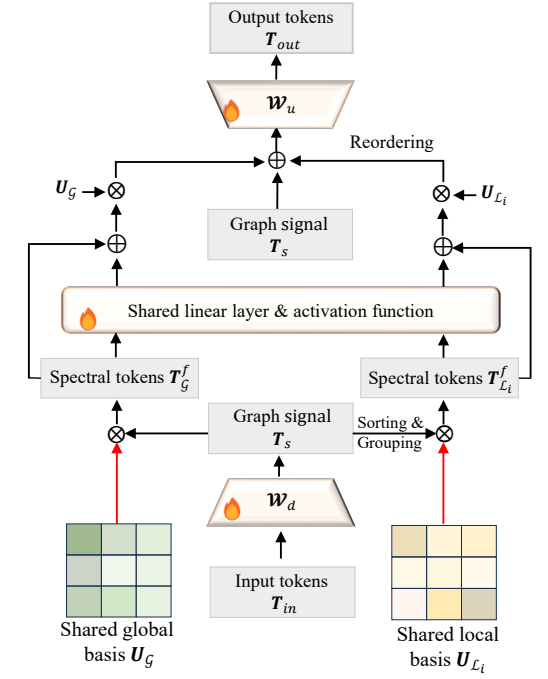
In our method, we associate graph vertices with key points in the point cloud, constructing the adjacency matrix \mathcal{W} considering the distances among these points.

4 METHOD

Fully fine-tuning a pre-trained point cloud model provides advanced performance, but substantial training costs accompany it. To address this challenge, we propose a novel method called PointGST, where the overall framework is illustrated in Fig. 2. Specifically, our method mainly consists of a regular pre-trained backbone and a series of lightweight Point Cloud Spectral Adapters (PCSA) integrated into each Transformer layer. During the fine-tuning, we keep the entire backbone frozen and only utilize a small number of trainable parameters (i.e., PCSA) to learn task-specific knowledge from the features of each instance. The PCSA transforms the point tokens from the spatial to the spectral domain, which de-correlates the inherent confusion of the point tokens from the frozen backbone. It efficiently fine-tunes fewer parameters for downstream tasks while introducing intrinsic information from the downstream point clouds for targeted tuning. As a result, it can significantly reduce the training cost and effectively connect the general knowledge from the pre-trained tasks with downstream tasks, leading to promising performance.



(a) The overall of our method



(b) The detail of our Point Cloud Spectral Adapter (PCSA)

Fig. 2: (a) The overall of our PointGST. During the fine-tuning phase, we freeze the given pre-trained backbones and only fine-tune the proposed lightweight Point Cloud Spectral Adapter (PCSA). (b) The details of our proposed PCSA. We treat the point tokens as graph signals and then transfer the point tokens from the spatial domain to the spectral domain for tuning. The PCSA is injected into each transformer layer in a parallel paradigm.

4.1 Transformer Encoder

Due to its flexible scalability, the Transformer encoder has become the predominant backbone for pre-training in point cloud analysis [4], [11], [47], [50], [85]. Specifically, after pre-processing steps such as Farthest Point Sampling (FPS) and Grouping, a lightweight PointNet is used to generate a series of point tokens ($\{t_i \in \mathbb{R}^{1 \times d} \mid 0 \leq i \leq n-1\}$), where d is the embedding dimension and n indicates the number of point patches. A classification token ($t_{cls} \in \mathbb{R}^{1 \times d}$) is then concatenated with these point tokens, forming $T_0 \in \mathbb{R}^{(n+1) \times d}$, which serves as the input to an L -layer Transformer. Each Transformer layer comprises an Attention module and a Feed-Forward Network (FFN), which are responsible for extracting token-to-token and channel-wise information, respectively:

$$\begin{aligned} T'_i &= \text{Attention}(\text{LN}(T_{i-1})) + T_{i-1}, \\ T_i &= \text{FFN}(\text{LN}(T'_i)) + T'_i, \end{aligned} \quad (6)$$

where $T_i \in \mathbb{R}^{(n+1) \times d}$ represents the output of the i -th layer, and LN denotes layer normalization. The Attention module and FFN are the most computationally and parameter-intensive components of the Transformer. In our approach, we keep the entire Transformer encoder frozen and inject the proposed learnable Point Cloud Spectral Adapter (PCSA) into the FFN in a parallel configuration.

4.2 Efficient Fine-Tuning in Spectral Domain

Compared with the spatial domain, the point tokens in the spectral domain can be easily de-correlated by distinct fre-

quency components. Fine-tuning the parameters in the spectral domain mitigates the confusion among tokens by using an orthogonal basis to separate them and provides compact intrinsic information from downstream point clouds. To achieve this, we introduce a simple and lightweight Point Cloud Spectral Adapter (PCSA) designed to learn task-specific knowledge in the spectral domain, as illustrated in Fig. 2(b). The spectral fine-tuning process is as follows:

- First, we transform the sampled n key points (for each point patch and point token) into multi-scale point cloud graphs, consisting of one global graph and k local sub-graphs. Subsequently, we generate the global Laplacian matrix L_G and the local Laplacian matrices L_L . By performing eigenvalue decomposition on L_G and L_L , we obtain two types of eigenvector matrix, termed U_G and U_L , respectively.
- Next, these eigenvector matrices (U_G and U_L) are shared across all frozen Transformer layers as the spectral basis for the Graph Fourier Transform (GFT). At each transformer layer, GFT is performed on the low-rank point tokens (serving as the graph signal) T_s with U_G and U_L to obtain global and local spectral domain tokens, respectively.
- Then, the proposed PCSA uses a shared linear layer to adapt the features. Following this, we recover the tokens to the spatial domain via inverse Graph Fourier Transform (iGFT) to align with the output of the transformer layer.

In the following contents, we elaborately describe how

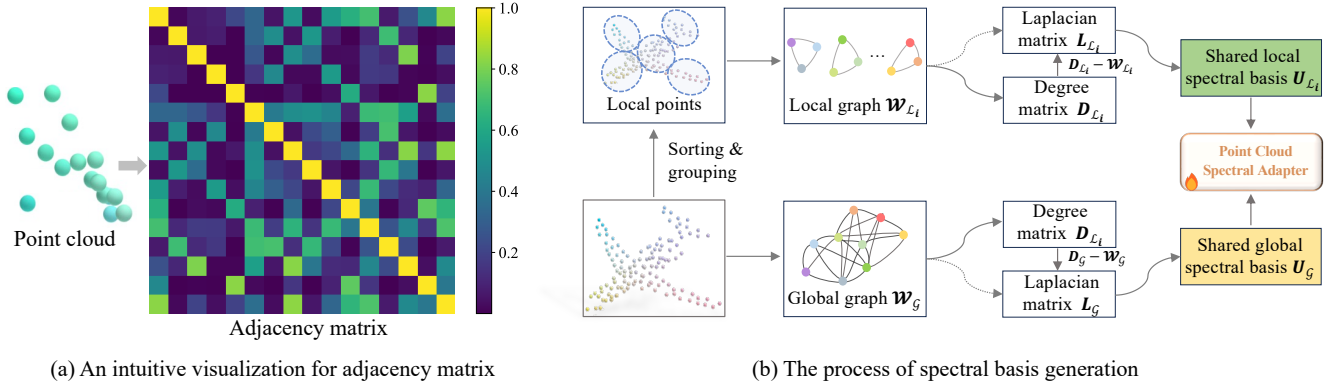


Fig. 3: (a) An intuitive visualization for our constructed graph, the adjacency matrix is symmetric, and the diagonal elements equal to 1. Smaller element values indicate greater geometric distances between point clouds. (b) The detailed process of our global and local spectral basis generation.

to fine-tune the parameters in the spectral domain.

4.2.1 From Point Cloud to Graph

To implement spectral tuning, we first opt to convert the point cloud into a customized point graph $\mathcal{G} = \{\mathcal{V}, \mathcal{E}, \mathbf{W}\}$ with vertices \mathcal{V} , edges \mathcal{E} and adjacency matrix $\mathbf{W} \in \mathbb{R}^{n \times n}$. An ideal \mathcal{G} should: **1)** Contain n vertices ($|\mathcal{V}| = n$) representing the n essential points in the point cloud. **2)** The element $w_{i,j}$ in \mathbf{W} quantifies the relationship between i -th and j -th points, where the highest self-correlation is reflected by the diagonal element. **3)** The relationship between points is influenced by their geometric properties, with closer point clouds exhibiting a stronger relationship.

Considering the design principles above, we calculate the relationship between the key points in a point patch. Then, we measure their pairwise distance to reflect the intrinsic information and capture the underlying structure. Specifically, we compute a point-pairwise distance matrix $\Delta \in \mathbb{R}^{n \times n}$, where each element $\delta_{i,j} \in \mathbb{R}$ represents the Euclidean distance between i -th and j -th points. However, such a distance matrix fails to meet principles **2)** and **3)**, e.g., the distance from the i -th point to itself is zero. Therefore, we further propose a simple data-dependent scaling strategy to define the adjacency matrix \mathbf{W} , and the element for i -th row and j -th column as follows:

$$w_{i,j} = \frac{1}{\frac{\delta_{i,j}}{\min(\Delta)} + \mathbf{I}_{i,j}}, \quad (7)$$

where $\min(\Delta) = \min(\delta_{i,j}), i \neq j$ represents the minimum value in Δ excluding zero, which varies across different samples and is data-dependent. $\mathbf{I} \in \mathbb{R}^{n \times n}$ is an identity matrix. Using the geometric locations of key points and a data-dependent scaling strategy, we construct a graph with weights based on a distance metric between the points, incorporating all the desired properties. An intuitive visualization of our constructed graph for a point cloud is present in Fig. 3(a).

4.2.2 Multi-Scale Point Cloud Graphs

To comprehensively capture the underlying structure in point clouds, we generate a series of graphs that enable the calculation of both global and local eigenvectors, as shown

in Fig. 3(b). Such an approach ensures a thorough usage of spectral features across different scales.

Global graph. We first treat all key points as an entirety and transform them into a global graph² \mathbf{W}_G . The details for translating the original point cloud to a graph are detailed in Sec. 4.2.1.

Local graph. We then propose constructing local sub-graphs from neighboring point clouds to capture the local structure by rearranging the n key points into k groups along a particular pattern. To be specific, the original key point set $\{p_0, \dots, p_{n-1}\}$ is scanned and sorted into $\{p'_0, \dots, p'_{n-1}\}$. This sorted set is then evenly divided into k groups, with each group containing m points, making $n = k \times m$. The i -th local point group can be defined as $\mathcal{L}_i = \{p'_{im}, \dots, p'_{(i+1)m-1} \mid 0 \leq i \leq k-1\}$. Based on this, we construct local sub-graphs for each group, resulting in $\{\mathbf{W}_{\mathcal{L}_0}, \dots, \mathbf{W}_{\mathcal{L}_i}, \dots, \mathbf{W}_{\mathcal{L}_{k-1}} \mid 0 \leq i \leq k-1\}$.

Both constructed global and local graphs effectively retain the intrinsic information of the original point cloud and underlying structure. These graphs subsequently will be used to generate the spectral basis, as detailed in the following subsection. Besides, the construction processing only needs to be implemented once for efficiency, i.e., the generated local and global graphs will be shared for all transformer layers.

4.2.3 Point Cloud Spectral Adapter

The proposed Point Cloud Spectral Adapter (PCSA) aims to convert the point tokens from the spatial to the spectral domain, and then effectively fine-tune the transformed signal, as shown in Fig. 2(b). Our PCSA is simple and extremely lightweight, as it just contains two matrices used for dimension adjustment and one shared linear layer used to fine-tune the spectral point tokens.

Down-projection. Let us denote the input tokens as $\mathbf{T}_{in} \in \mathbb{R}^{n \times C}$, where C is the input dimension. Here, we omit the class token and refer to \mathbf{T}_{in} as the n point tokens in this section. Our PCSA begins with a downward projection

²For simplicity, we directly utilize the adjacency matrix to represent a graph.

using trainable parameters $\mathbf{W}_d \in \mathbb{R}^{r \times C}$, with $r \ll C$. The low-rank graph signal \mathbf{T}_s are obtained by:

$$\mathbf{T}_s = \mathbf{T}_{in} \mathbf{W}_d^\top, \quad (8)$$

where $\mathbf{T}_s \in \mathbb{R}^{n \times r}$ provides a general representation of point patches. The n point patches are embedded by the corresponding n key points with their neighbors, enabling \mathbf{T}_s to function as a graph signal with the key points as vertices. The \mathbf{T}_s is also rearranged into k local graph signal, as mentioned in Sec. 4.2.2, resulting in $\mathbf{T}_s^{\mathcal{L}_i} \in \mathbb{R}^{m \times r}$ ($0 \leq i \leq k-1$), corresponding to the key points in \mathcal{L}_i . Also, the \mathbf{T}_s can serve as the global graph signal notated as $\mathbf{T}_s^{\mathcal{G}} \in \mathbb{R}^{n \times r}$.

Spectral basis generation. After the down-projection, the graph signal \mathbf{T}_s still remains in the spatial domain. Two preparations are required before applying Graph Fourier Transform (GFT) in the spatial point clouds, first to compute the Laplacian matrix $\mathbf{L}_G \in \mathbb{R}^{n \times n}$ and $\mathbf{L}_{\mathcal{L}_i} \in \mathbb{R}^{m \times m}$ for the constructed the global graph $\mathbf{W}_G \in \mathbb{R}^{n \times n}$ and local sub-graphs $\mathbf{W}_{\mathcal{L}_i} \in \mathbb{R}^{m \times m}$, respectively. We then perform eigenvalue decomposition to generate the spectral basis for the GFT and its inverse, as shown in Fig. 3(b).

For simplicity, the following content uses the global spectral for illustration. Specifically, we first produce the diagonal degree matrix \mathbf{D}_G for the global graph \mathbf{W}_G :

$$d_{i,j} = \begin{cases} \sum_{l=0}^{n-1} w_{i,l} & , i=j \\ 0 & , i \neq j \end{cases}, \quad (9)$$

where each entry $d_{i,i}$ indicates the sum of the weights on connected edges for each node (key point). Based on \mathbf{D}_G , the graph Laplacian matrix is represented as $\mathbf{L}_G = \mathbf{D}_G - \mathbf{W}_G$. The constructed graphs contain real and non-negative edge weights, making \mathbf{L}_G a real, symmetric, and positive semi-definite matrix [8]. Therefore, \mathbf{L}_G can be decomposed as:

$$\mathbf{L}_G = \mathbf{U}_G \mathbf{\Lambda}_G \mathbf{U}_G^\top, \quad (10)$$

where $\mathbf{U}_G = [\mathbf{u}_0, \dots, \mathbf{u}_{n-1}] \in \mathbb{R}^{n \times n}$ is an orthogonal matrix of eigenvectors \mathbf{u}_i , formed as a set of spectral basis for spectral domain. Similarly, we can also obtain the Laplacian matrix $\mathbf{L}_{\mathcal{L}_i}$ and $\mathbf{U}_{\mathcal{L}_i} \in \mathbb{R}^{m \times m}$ for the local sub-graph $\mathbf{W}_{\mathcal{L}_i}$. The \mathbf{U}_G and $\mathbf{U}_{\mathcal{L}_i}$ are computed only once and shared across all transformer layers.

Graph Fourier Transform. We then perform a matrix multiplication of low-dimensional token (graph signal) \mathbf{T}_s with spectral basis \mathbf{U}_G and $\mathbf{U}_{\mathcal{L}_i}$ to represent the graph signal in the spectral domain. Specifically, for the global graph signal \mathbf{T}_s , we apply GFT by multiplying it with the global basis \mathbf{U}_G to output \mathbf{T}_G^f , derive global spectral information. Similarly, the i -th local graph signal $\mathbf{T}_s^{\mathcal{L}_i}$ will multiply with the local basis $\mathbf{U}_{\mathcal{L}_i}$, resulting in $\mathbf{T}_{\mathcal{L}_i}^f$:

$$\mathbf{T}_G^f = \text{GFT}(\mathbf{T}_s) = \mathbf{U}_G^\top \mathbf{T}_s, \quad \mathbf{T}_{\mathcal{L}_i}^f = \text{GFT}(\mathbf{T}_s^{\mathcal{L}_i}) = \mathbf{U}_{\mathcal{L}_i}^\top \mathbf{T}_s^{\mathcal{L}_i}. \quad (11)$$

Next, all tokens are passed through a shared linear layer featuring a residual connection:

$$\mathbf{T}_G^{f'} = \mathbf{T}_G^f + \text{act}(\text{Linear}(\mathbf{T}_G^f)), \quad \mathbf{T}_{\mathcal{L}_i}^{f'} = \mathbf{T}_{\mathcal{L}_i}^f + \text{act}(\text{Linear}(\mathbf{T}_{\mathcal{L}_i}^f)), \quad (12)$$

where the act refers to the Swish activation function [53]. We initialize the linear layer to zero during the initial stages for stable training.

Inverse Graph Fourier Transform. To align with the output of the transformer layer, these tuned tokens $\mathbf{T}_{\mathcal{L}_i}^{f'}$ and

$\mathbf{T}_G^{f'}$ in the spectral domain will be further transformed back to the spatial domain via the inverse GFT (iGFT):

$$\hat{\mathbf{T}}_G^f = \text{iGFT}(\mathbf{T}_G^{f'}) = \mathbf{U}_G \mathbf{T}_G^{f'}, \quad \hat{\mathbf{T}}_{\mathcal{L}_i}^f = \text{iGFT}(\mathbf{T}_{\mathcal{L}_i}^{f'}) = \mathbf{U}_{\mathcal{L}_i} \mathbf{T}_{\mathcal{L}_i}^{f'}, \quad (13)$$

where both $\hat{\mathbf{T}}_G^f$ and $\hat{\mathbf{T}}_{\mathcal{L}_i}^f$ are the converted spatial tokens. It should be noted that due to the introduced sorting and grouping strategy, the tokens of local spectral represent point cloud patches that do not align with the backbone part. Therefore, it is necessary to reorder the spatial local tokens to match the order of \mathbf{T}_s . Specifically, we concatenate the $\mathbf{T}_{\mathcal{L}_i}^f$ of all sub-graphs and reordered it, resulting in the tokens $\hat{\mathbf{T}}_{\mathcal{L}}^f \in \mathbb{R}^{n \times r}$:

$$\hat{\mathbf{T}}_{\mathcal{L}}^f = \text{reorder}(\text{concat}[\hat{\mathbf{T}}_{\mathcal{L}_0}^f, \dots, \hat{\mathbf{T}}_{\mathcal{L}_{k-1}}^f]). \quad (14)$$

Up-projection and output. The PCSA finally employs a zero-initialized upward projection matrix $\mathbf{W}_u \in \mathbb{R}^{C \times r}$ and a manual scale $s \in \mathbb{R}$ to restore the fine-tuned compressed representations to the dimensions processed by the backbone:

$$\mathbf{T}_{out} = s \times (\text{act}(\mathbf{T}_s) + \hat{\mathbf{T}}_G^f + \hat{\mathbf{T}}_{\mathcal{L}}^f) \mathbf{W}_u^\top, \quad (15)$$

where the output of the proposed point cloud spectral adapter \mathbf{T}_{out} is added back to the FFN of the transformer block, as shown in Fig. 2(a).

Through the PCSA, we successfully fine-tune the parameter in the spectral domain, effectively transferring the general knowledge to the downstream tasks.

4.3 Theoretical Analysis

4.3.1 Insight of applying Graph Fourier Transform in PEFT

We summarize applying Graph Fourier Transform in PEFT into twofold: 1) The Graph Fourier Transform (GFT) conducts a signal decorrelation, resulting in a compact representation in the spectral domain. 2) Tuning in the spectral domain actually adjusts the “energy” of each graph frequency for the graph signal.

For discrete signals like point clouds, the graph Laplacian matrices can be considered as precision matrices within Gaussian-Markov Random Fields (GMRFs) [57]. This probabilistic perspective shows that the GFT approximates the Karhunen-Loève Transform (KLT) for signal decorrelation in GMRFs. Previous studies [12], [89], [90] also indicate that the GFT is an approximately optimal linear transform for decorrelating signals, which aids in geometric data compression. Since the GFT approximates the KLT for optimal signal decorrelation across various statistical processes, tuning in this domain is efficient and explicit.

Besides, our method for generating customized point graphs considers the relationship between points and adapts to the topology of point clouds, thereby injecting intrinsic knowledge of downstream tasks into the GFT process. By adopting the GFT, we can define the $\alpha_i = \mathbf{u}_i^\top \mathbf{T}$, where $\mathbf{u}_i \in \mathbb{R}^{1 \times n}$ is the i -th eigenvector and $\mathbf{T} \in \mathbb{R}^{n \times r}$ is the graph signal. The term $|\alpha_i|^2$ is commonly referred to as the “energy” at the i -th graph frequency (corresponding to the k -th eigenvalue λ_i of the Laplacian matrix) for signal \mathbf{T} . In other words, the shared linear layer in the Point Cloud Spectral Adapter (PCSA) adjusts α_i at each frequency,

TABLE 1: The comparison of our PointGST and baseline methods in terms of storage usage when fine-tuning various downstream point cloud datasets or tasks.

Method	OBJ_BG	OBJ_ONLY	PB_T50_RS	ModelNet40	ModelNet Few-shot	ShapeNetPart	S3DIS	Total
Point-MAE [47]	22.1M	22.1M	22.1M	22.1M	22.1M	27.1M	27.0M	164.6M
PointGST (ours)	0.6M	0.6M	0.6M	0.6M	0.6M	5.6M	5.6M	14.2M
PointGPT-L [4]	360.5M	360.5M	360.5M	360.5M	360.5M	389.9M	389.9M	2582.3M
PointGST (ours)	2.4M	2.4M	2.4M	2.4M	2.4M	31.9M	31.9M	75.8M

allowing our PointGST to implement a direct and effective fine-tuning paradigm.

Based on the above perceptions, we argue that the proposed PCSA can supplement the inner informed features from the fixed branch with explicit knowledge directly from point clouds for better feature integration. Specifically, the downward project W_d generates a low-ranked feature for each point patch, which acts as graph signals with key points as vertices. Additionally, the residual connection and zero-initialized strategy in our PCSA ensure training stability. The experiments in the following sections will validate the effectiveness and robustness of our architecture.

4.3.2 Training Cost

Our method requires only fine-tuning the proposed lightweight Point Cloud Spectral Adapter (PCSA) while freezing the entire pre-trained backbone. Specifically, the GFT and iGFT operations do not introduce extra parameters, while each Spectral Adapter module adds only $2 \times r \times d$ from W_d/W_u , and $r \times r$ from the shared tuning Linear as trainable parameters (bias and layer normalization are ignored). The intermediate dimension r is relatively small compared to d . For example, we only need to fine-tune about 0.6% of the parameters in the SOTA baseline, PointGPT-L [4], achieving promising results.

As the amount of downstream tasks or datasets requiring fine-tuning increases, we only need to store the task/dataset-specific PCSA and one original pre-trained models. As shown in Tab. 1, when fine-tuning various downstream tasks, our PointGST significantly compresses model size compared to the baselines (Point-MAE [47] and PointGPT-L [4]).

We further analyze the training GPU memory, which is an important metric for evaluating the training cost of a neural network. As shown in Fig. 4, our method significantly reduces training memory as the batch size increases compared with Point-MAE [47]. In addition, compared with the previous representative PEFT methods for point cloud [88], [99], we present clear advantages, especially under the widely-used batch sizes such as 16 and 32.

5 EXPERIMENTS SETUP

This section describes the implementation details and the comparison methods.

5.1 Datasets and Implement Details

All the experiments are conducted on a single NVIDIA 3090 GPU. During fine-tuning, the parameters of the pre-trained backbones remain frozen, while only the newly

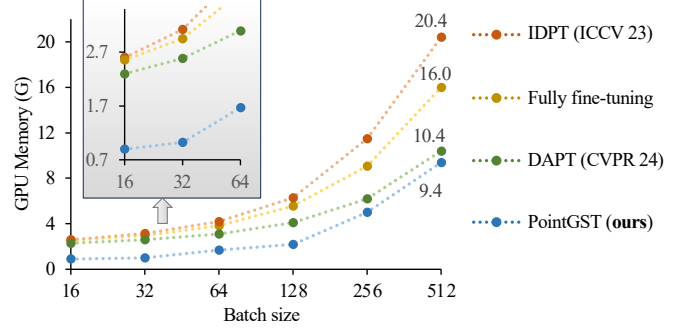


Fig. 4: The comparison of used training GPU memory.

added parameters are updated. The hyper-parameters k and r are set to 4 and 36, respectively. We employ a transpose format of Z space-filling curve [46] to scan the key points to construct the local graphs. This subsection introduces the implementation details along with the dataset.

ScanObjectNN [68] is a challenging 3D real-world objects dataset, consisting of $\sim 15K$ indoor object point cloud instances, across 15 categories. There are three widely used variants, including OBJ_BG, OBJ_ONLY, and PB_T50_RS, each with increasing complexity. The training setup is aligned with the compared baseline. Specifically, we employ the AdamW optimizer [41] with a weight decay of 0.05 and a cosine learning rate scheduler [42], starting with an initial learning rate of $5e-4$ and a 10-epoch warm-up. The model is trained for 300 epochs with a batch size of 32. For consistency, we utilize 2048 points in the point cloud, divided into 128 groups of 32 points each.

ModelNet40 [79] is a commonly used synthesis 3D point cloud dataset that contains 12,311 CAD models of 40 categories. The network training settings follow ScanObjectNN. The input point cloud consists of 1,024 points, divided into 64 groups with 32 points per group.

ShapeNetpart [83] is a popular point-level synthetic object part segmentation benchmark that includes 16,881 instances across 16 object categories and 50 part categories. We use the AdamW optimizer with a weight decay of $1e-4$ and the cosine learning rate scheduler, with an initial learning rate of $1e-4$ and a 10-epoch warm-up. The models are trained for 300 epochs with a batch size of 16, using 2048 input points divided into 128 groups of 32 points each.

S3DIS [2] comprises six large-scale indoor areas, covering 273 million points from 13 categories. Following previous work [65], we advocate using Area 5 for evaluation purposes for better and fair generalization performance benchmarking. The cosine learning rate scheduler with an initial learning rate of $2e-4$ is applied. We train our model

TABLE 2: The comparison between other fine-tuning strategies and our PointGST. We report the overall accuracy (OA) and trainable parameters (Params.) across three variants of ScanObjectNN [68] and ModelNet40 [79]. All methods use default data augmentation as the baseline. * indicates reproduced results. ScanObjectNN results are reported without voting, while ModelNet40 results are presented both with and without voting (-/-).

Pre-trained model	Fine-tuning strategy	Reference	Params. (M)	FLOPs (G)	ScanObjectNN			ModelNet40	
					OBJ_BG	OBJ_ONLY	PB_T50_RS	OA (%)	
Point-BERT [85] (CVPR 22)	Fully fine-tune	-	22.1 (100%)	4.76	87.43	88.12	83.07	92.7 / 93.2	
	IDPT [88]	ICCV 23	1.7 (7.69%)	7.10	88.12(+0.69)	88.30(+0.18)	83.69(+0.62)	92.6(-0.1) / 93.4(+0.2)	
	Point-PEFT [64]	AAAI 24	0.7 (3.13%)	-	-	-	85.00(+1.93)	93.4(+0.7) / -	
	DAPT [99]	CVPR 24	1.1 (4.97%)	4.96	91.05(+3.62)	89.67(+1.55)	85.43(+2.36)	93.1(+0.4) / 93.6(+0.4)	
	PointGST (ours)	-	0.6 (2.77%)	4.81	91.39(+3.96)	89.67(+1.55)	85.64(+2.57)	93.4(+0.7) / 93.8(+0.6)	
Point-MAE [47] (ECCV 22)	Fully fine-tune	-	22.1 (100%)	4.76	90.02	88.29	85.18	93.2 / 93.8	
	IDPT [88]	ICCV 23	1.7 (7.69%)	7.10	91.22(+1.20)	90.02(+1.73)	84.94(-0.24)	93.3(+0.1) / 94.4(+0.6)	
	DAPT [99]	CVPR 24	1.1 (4.97%)	4.96	90.88(+0.86)	90.19(+1.90)	85.08(-0.10)	93.5(+0.3) / 94.0(+0.2)	
	PointGST (ours)	-	0.6 (2.77%)	4.81	91.74(+1.72)	90.19(+1.90)	85.29(+0.11)	93.5(+0.3) / 94.0(+0.2)	
ACT [11] (ICLR 23)	Fully fine-tune	-	22.1 (100%)	4.76	93.29	91.91	88.21	- / 93.7	
	IDPT [88]	ICCV 23	1.7 (7.69%)	7.10	93.12(-0.17)	92.26(+0.35)	87.65(-0.56)	- / 94.0(+0.3)	
	DAPT* [99]	CVPR 24	1.1 (4.97%)	4.96	92.60(-0.69)	91.57(-0.34)	87.54(-0.67)	92.7 / 93.2(-0.5)	
	PointGST (ours)	-	0.6 (2.77%)	4.81	93.46(+0.17)	92.60(+0.69)	88.27(+0.06)	93.4 / 94.0(+0.3)	
RECON [50] (ICML 23)	Fully fine-tune	-	22.1 (100%)	4.76	94.32	92.77	90.01	92.5 / 93.0	
	IDPT* [88]	ICCV 23	1.7 (7.69%)	7.10	93.29(-1.03)	91.57(-1.20)	87.27(-2.74)	93.4(+0.9) / 93.5(+0.5)	
	DAPT [99]	CVPR 24	1.1 (4.97%)	4.96	94.32(-0.00)	92.43(-0.34)	89.38(-0.63)	93.5(+1.0) / 94.1(+1.1)	
	PointGST (ours)	-	0.6 (2.77%)	4.81	94.49(+0.17)	92.94(+0.17)	89.49(-0.52)	93.6(+1.1) / 94.1(+1.1)	
PointGPT-L [4] (NeurIPS 23)	Fully fine-tune	-	360.5 (100%)	67.71	97.2	96.6	93.4	94.1 / 94.7	
	IDPT* [88]	ICCV 23	10.0 (2.77%)	75.19	98.11(+0.91)	96.04(-0.56)	92.99(-0.41)	93.4(-0.7) / 94.6(-0.1)	
	DAPT* [99]	CVPR 24	4.2 (1.17%)	71.64	98.11(+0.91)	96.21(-0.39)	93.02(-0.38)	94.2(+0.1) / 94.9(+0.2)	
	PointGST (ours)	-	2.4 (0.67%)	67.95	98.97(+1.77)	97.59(+0.99)	94.83(+1.43)	94.8(+0.7) / 95.3(+0.6)	

for 60 epochs with a batch size of 32. Other configurations are the same as ShapeNetpart.

5.2 Compared Methods

To illustrate the effectiveness of our approach, popular pre-train models like Point-BERT [85], Point-MAE [47], ACT [11], RECON [50], and PointGPT [4] are selected as our baselines. Additionally, we include the SOTA point cloud PEFT methods for comparisons: 1) IDPT [88] utilizes DGCNN [74] to generate instance-aware prompts before the last transformer layer for model fine-tuning rather than relying on static prompts; 2) Point-PEFT [64] utilize a point-prior bank for feature aggregation and incorporating Adapters into each transformer block. 3) DA [15] uses a dynamic aggregation method to replace previous static aggregation for pre-trained point cloud Transformers. 4) DAPT [99], the latest SOTA point cloud PEFT method, proposes to adjust tokens based on significance scores.

It is important to note that among the methods mentioned above, IDPT and DAPT conduct more comprehensive experiments compared to the other two approaches. As a result, we primarily follow the experimental setups of IDPT and DAPT to organize our experiments.

6 RESULTS AND ANALYSIS

In this section, we conduct experiments to show the effectiveness of our approach.

TABLE 3: Classification on ScanObjectNN PB_T50_RS [68] with strong data augmentation. Overall accuracy (%) without voting is reported. Params. is the trainable parameters.

Pre-trained model	Fine-tuning strategy	Reference	Params. (M)	PB_T50_RS
Point-MAE [40] (ECCV 22)	Fully fine-tune	-	22.1	88.4
	DA [15]	ICRA 24	1.6	88.0
	Point-PEFT [64]	AAAI 24	0.7	89.1
	PointGST (ours)	-	0.6	89.3

6.1 3D Classification

6.1.1 The comparisons of different fine-tuning strategies

We first comprehensively compare the representative fine-tuning strategies used in the point cloud tasks, including the fully fine-tuning (FFT), IDPT [88], and DAPT [99], in terms of trainable parameters (Params.) and performance. We apply our PointGST to various pre-trained models, such as Point-BERT [85], Point-MAE [47], ACT [11], RECON [50], and PointGPT-L [4], size ranging from 22.1M to 360.5M. Tab. 2 lists the detailed results, and it can find that:

1) **PointGST effectively balances the number of trainable parameters and performance.** Based on the quantitative comparisons, it is evident that increasing the scale of a pre-trained model will improve the performance. However, this would meanwhile come at a huge cost of fine-tuning, e.g., Point-MAE and PointGPT-L report 85.18% and 93.4% with 22.1M and 360.5M parameters on the ScanObjectNN PB_T50_RS dataset, respectively. Thanks to only fine-tuning a few parameters in the spectral domain, our method can effectively address this dilemma. Specifically, on the most convincing pre-trained point cloud models, PointGPT-L,

TABLE 4: Comparison of overall accuracy (OA) and trainable parameters (Params.) across three variants of ScanObjectNN [68] and ModelNet40 [79]. Results highlighted in green indicate the use of the voting strategy.

Method	Reference	Params. (M)	ScanObjectNN			ModelNet40	
			OBJ_BG	OBJ_ONLY	PB_T50_RS	Points Num.	OA (%)
Supervised Learning Only							
PointNet [48]	CVPR 17	3.5	73.3	79.2	68.0	1k	89.2
PointNet++ [49]	NeurIPS 17	1.5	82.3	84.3	77.9	1k	90.7
DGCNN [74]	TOG 19	1.8	82.8	86.2	78.1	1k	92.9
MVTN [20]	ICCV 21	11.2	-	-	82.8	1k	93.8
3D-GCN [38]	TPAMI 22	-	-	-	-	1k	92.1
RepSurf-U [55]	CVPR 22	1.5	-	-	84.3	1k	94.4
PointNeXt [52]	NeurIPS 22	1.4	-	-	87.7	1k	94.0
PTv2 [78]	NeurIPS 22	12.8	-	-	-	1k	94.2
PointMLP [44]	ICLR 22	13.2	-	-	85.4	1k	94.5
PointMeta [37]	CVPR 23	-	-	-	87.9	-	-
ADS [22]	ICCV 23	-	-	-	87.5	1k	95.1
X-3D [61]	CVPR 24	5.4	-	-	90.7	-	-
GPSFormer [72]	ECCV 24	2.4	-	-	95.4	1k	94.2
Self-Supervised Representation Learning (Full fine-tuning)							
OcCo [73]	ICCV 21	22.1	84.85	85.54	78.79	1k	92.1
Point-BERT [85]	CVPR 22	22.1	87.43	88.12	83.07	1k	93.2
MaskPoint [40]	ECCV 22	22.1	89.70	89.30	84.60	1k	93.8
Point-MAE [47]	ECCV 22	22.1	90.02	88.29	85.18	1k	93.8
Point-M2AE [93]	NeurIPS 22	15.3	91.22	88.81	86.43	1k	94.0
ACT [11]	ICLR 23	22.1	93.29	91.91	88.21	1k	93.7
RECON [50]	ICML 23	43.6	94.15	93.12	89.73	1k	93.9
PointGPT-L [4]	NeurIPS 23	360.5	97.2	96.6	93.4	1k	94.7
Point-FEMAE [87]	AAAI 24	27.4	95.18	93.29	90.22	1k	94.5
P2P++ [75]	TPAMI 24	16.1	-	-	90.3	1k	94.1
PointDif [98]	CVPR 24	-	93.29	91.91	87.61	-	-
PointMamba [36]	NeurIPS 24	12.3	94.32	92.60	89.31	-	-
MH-PH [16]	ECCV 24	-	97.4	96.8	93.8	1k	94.6
RECON++-L [51]	ECCV 24	657.2	98.80	97.59	95.25	1k	94.8
Self-Supervised Representation Learning (Efficient fine-tuning)							
PointGST (ours)	-	2.4	98.97	97.59	94.83	1k	94.8
PointGST (ours)	-	2.4	99.48	97.76	96.18	1k	95.3

compared with the fully fine-tuning (FFT), we only need 2.4M trainable parameters, which is merely 0.6% of the FFT. More importantly, with so few training parameters, we even outperform the FFT by 1.77%, 0.99%, 1.43%, and 0.7% on the OBJ_BG, OBJ_OBLY, PB_T50_RS and ModelNet40 datasets, respectively.

Compared to spatial domain-based methods like IDPT and DAPT, our PointGST achieves superior performance with fewer trainable parameters by leveraging the spectral domain, where features are more easily de-correlated. In addition, our PointGST introduces intrinsic information via the Graph Fourier Transform (GFT), enabling targeted fine-tuning. In short, PointGST proves to be a potential candidate that brings promising performance and parameter-efficient approaches to low-resource scenarios.

2) PointGST can effectively generalize to diverse pre-trained models. A good PEFT method should consistently perform well across different pre-trained models, regardless of the pre-training strategies, data used, or model sizes. However, our observations reveal that existing PEFT methods [15], [64], [88], [99] fail to deliver consistent improvements across diverse pre-trained models. For instance, as shown in Tab. 2, we apply five distinct pre-trained models,

varying in pre-training techniques (e.g., masked modeling and contrastive learning) and sizes (ranging from 22.1M to 360.5M parameters). Notably, both IDPT and DAPT exhibit negative impacts when applied to baselines like ACT and RECON. Even in scenarios where these methods produce positive outcomes, the gains from IDPT and DAPT remain limited. In contrast, our PointGST consistently yields improvements across most conducted pre-trained models and outperforms IDPT and DAPT.

In addition, we find that both Point-PEFT [64] and DA [15] apply the point cloud rotation as the data augmentation [11] on the Point-MAE. To keep fair, we also adopt the augmentations to conduct experiments. The comparisons in Tab. 3 clearly show that PointGST consistently achieves higher accuracy than Point-PEFT and DA.

6.1.2 Compared with state-of-the-art methods

The comparisons between the state-of-the-art (SOTA) methods and our proposed method on ScanObjectNN and ModelNet40 are illustrated in Tab. 4. We categorize the comparison methods into two types: supervised learning only and self-supervised representation learning with full fine-

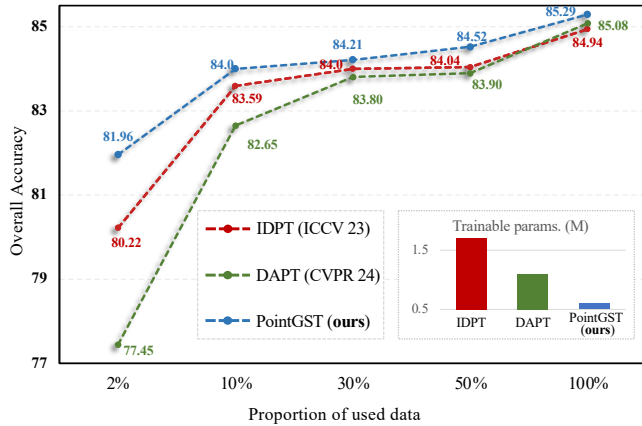


Fig. 5: Few-shot training performance on the ScanObjectNN PB_T50_RS dataset at different training data proportions.

tuning. The results yield two notable observations regarding the efficacy of the proposed PointGST:

1) Self-supervised representation learning methods [4], [11], [50] generally outperform those based solely on supervised learning [22], [44], [55], emphasizing the critical role of pre-training. Additionally, these self-supervised methods often involve more trainable parameters than their supervised counterparts (e.g., 13.2M and 657.2M for PointMLP [44] and RECON++-L [51], respectively), which underscores the practical relevance of parameter-efficient fine-tuning.

2) When using PointGPT-L [4] as the baseline, our PointGST outperforms all previous methods, establishing a new state-of-the-art, while requiring only 2.4M trainable parameters. To the best of our knowledge, this is the first approach to nearly saturate the performance on the ScanObjectNN OBJ_BG dataset (e.g., 99.48% OA). Note that it is not something that can be brought about by simply fitting a dataset. Instead, it highlights the current limitations of existing point cloud analysis datasets in effectively evaluating new methods. Consequently, we encourage the community to develop more challenging datasets to better assess the progress in future point cloud analysis research.

6.2 Few-shot Learning

Few-shot learning plays a crucial role in evaluating the efficiency of data usage for training. We make few-shot comparisons on ModelNet40 and the results are listed in Tab. 5. Our PointGST beats the previous PEFT methods [88], [99] in all conducted settings. To further verify the few-shot training ability of our method, we conducted experiments on the challenging ScanObjectNN PB_T50_RS dataset, where we set the range from 2% to 100%, as depicted in Fig. 5. Specifically, our PointGST demonstrates strong robustness when trained on limited data. Especially with only 2% of the training data, PointGST achieves an overall accuracy of 81.96%, significantly outperforming IDPT [88] and DAPT [99] by 1.74% and 4.51%, respectively. In addition, we report the least trainable parameters, only 0.6M. The results indicate that PointGST efficiently leverages limited training data to capture the underlying characteristics of point clouds, outperforming existing point cloud PEFT methods, particularly in data-constrained environments.

TABLE 5: Few-shot learning on ModelNet40 [79]. Overall accuracy \pm standard deviation without voting is reported.

Methods	Reference	5-way		10-way	
		10-shot	20-shot	10-shot	20-shot
<i>with Self-Supervised Representation Learning (Full fine-tuning)</i>					
MaskPoint [40]	ECCV 22	95.0±3.7	97.2±1.7	91.4±4.0	93.4±3.5
Point-M2AE [93]	NeurIPS 22	96.8±1.8	98.3±1.4	92.3±4.5	95.0±3.0
ACT [11]	ICLR 23	96.8±2.3	98.0±1.4	93.3±4.0	95.6±2.8
PointGPT-L [4]	NeurIPS 23	98.0±1.9	99.0±1.0	94.1±3.3	96.1±2.8
RECON++-L [51]	ECCV 24	98.0±2.3	99.5±0.8	94.5±4.1	96.5±3.0
<i>with Self-Supervised Representation Learning (Efficient fine-tuning)</i>					
Point-BERT [85] (baseline)	CVPR 22	94.6±3.1	96.3±2.7	91.0±5.4	92.7±5.1
+ IDPT [88]	ICCV 23	96.0±1.7	97.2±2.6	91.9±4.4	93.6±3.5
+ DAPT [99]	CVPR 24	95.8±2.1	97.3±1.3	92.2±4.3	94.2±3.4
+ PointGST (ours)	-	96.5±2.4	97.9±2.0	92.7±4.2	95.0±2.8
Point-MAE [47] (baseline)	ECCV 22	96.3±2.5	97.8±1.8	92.6±4.1	95.0±3.0
+ IDPT [88]	ICCV 23	97.3±2.1	97.9±1.1	92.8±4.1	95.4±2.9
+ DAPT [99]	CVPR 24	96.8±1.8	98.0±1.0	93.0±3.5	95.5±3.2
+ PointGST (ours)	-	98.0±1.8	98.3±0.9	93.7±4.0	95.7±2.4

TABLE 6: Part segmentation on the ShapeNetPart [83]. The mIoU for all classes (Cls.) and for all instances (Inst.) are reported. Params. represents the trainable parameters. * denotes reproduced results.

Methods	Reference	Params. (M)	Cls. mIoU (%)	Inst. mIoU (%)
Point-BERT [85] (baseline)	CVPR 22	27.06	84.11	85.6
+ IDPT* [88]	ICCV 23	5.69	83.50	85.3
+ Point-PEFT* [64]	AAAI 24	5.62	81.12	84.3
+ DAPT [99]	CVPR 24	5.65	83.83	85.5
+ PointGST (ours)	-	5.58	83.87	85.7
Point-MAE [47] (baseline)	ECCV 22	27.06	84.19	86.1
+ IDPT [88]	ICCV 23	5.69	83.79	85.7
+ Point-PEFT* [64]	AAAI 24	5.62	83.20	85.2
+ DAPT [99]	CVPR 24	5.65	84.01	85.7
+ PointGST (ours)	-	5.59	83.81	85.8
RECON [50] (baseline)	ICML 23	27.06	84.52	86.1
+ IDPT* [88]	ICCV 23	5.69	83.66	85.7
+ Point-PEFT* [64]	AAAI 24	5.62	83.10	85.1
+ DAPT [99]	CVPR 24	5.65	83.87	85.7
+ PointGST (ours)	-	5.59	83.98	85.8

6.3 Part Segmentation

Part segmentation presents challenges in accurately predicting detailed class labels for each point. Following DAPT [99], we apply the Point-BERT, Point-MAE, and RECON as baselines on the ShapeNetPart dataset. We incorporated the proposed point cloud spectral adapter (PCSA) into every layer of the models. The quantitative results are shown in Tab. 6. Our method achieves highly competitive performance while utilizing significantly fewer trainable parameters than fully fine-tuning counterparts (i.e., baseline methods). Notably, the increase in trainable parameters is mainly due to the head part, but we still reduce overall trainable parameters and surpass the performance of other PEFT methods like IDPT [88], Point-PEFT [64] and DAPT [99].

6.4 Scene-level Point Cloud Analysis

We evaluate the proposed PointGST on the semantic segmentation task using the S3DIS dataset [2], with results shown in Tab. 7. Our empirical observations suggest that previous PEFT methods [64], [88], [99] struggle with this task, likely due to the models being pre-trained on object-level datasets [3]. This results in sub-optimal performance

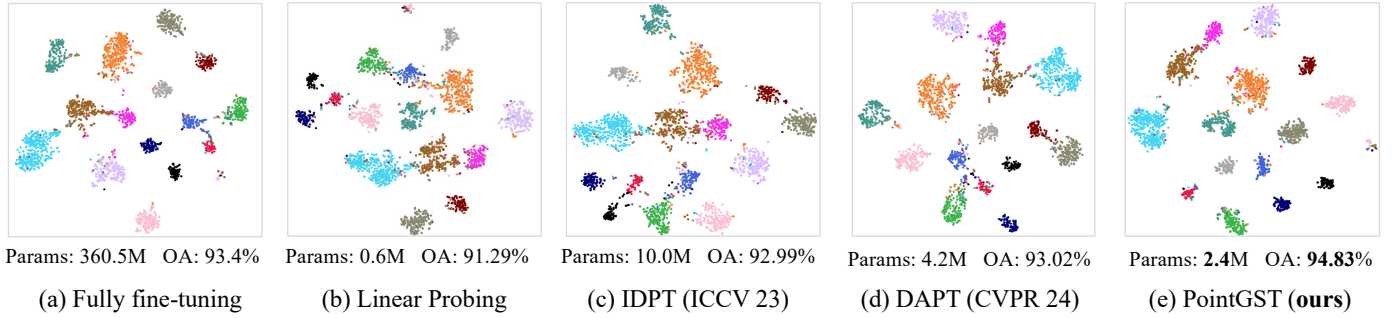


Fig. 6: The t-SNE visualizations, along with the trainable parameters (Params.) and overall accuracy (OA), are derived from the ScanObjectNN PB_T50_RS dataset using a pre-trained PointGPT-L with various tuning strategies. The final classification features for t-SNE visualizations are extracted from the last linear layer.

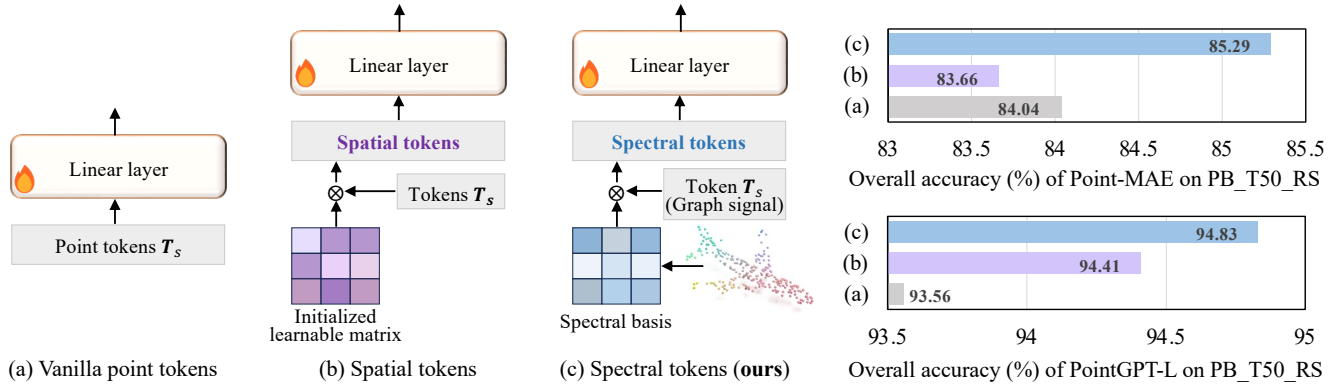


Fig. 7: (a) Default point tokens T_s . (b) Initializing a learnable matrix to act on T_s , still in the spatial domain. (c) The proposed method transfers the T_s (graph signal) to the spectral tokens.

when fine-tuned on a scene-level dataset. In contrast, the proposed PointGST effectively utilizes intrinsic information during fine-tuning, bridging the performance gap between fully and efficiently fine-tuning strategies. For example, using ACT [11] as the baseline, PointGST achieves 67.6% mAcc and 57.4% mIoU with only 5.55M trainable parameters, substantially outperforming IDPT [88], Point-PEFT [64] and DAPT [99] by 3.5%/5.3%, 1.6%/2.8%, and 3.5%/2.9% in mAcc/mIoU, respectively. Similarly, when applied to PointMAE [47] and RECON [50], PointGST consistently surpasses both IDPT, Point-PEFT, and DAPT, further demonstrating its robustness across different pre-trained models.

6.5 Compared with PEFT methods from other domains

The provided Tab. 8 presents a comparative analysis of various PEFT methods originating from natural language processing (NLP) and 2D vision. The results clearly show that although PEFT methods in other areas can be adapted for 3D tasks, their performance falls short compared to methods specifically designed for 3D vision. For instance, the best-performing PEFT methods from NLP and 2D vision achieve overall accuracies of 83.93% and 83.66%, respectively, leaving a significant performance gap compared to fully fine-tuning, which achieves 85.18%. This indicates the need for 3D-specific adaptations or entirely new methods tailored to 3D data. The existing point cloud PEFT methods, IDPT [88] and DAPT [99], show better performance with accuracies of 84.94% and 85.08%, respectively. However, their

TABLE 7: Semantic segmentation on the S3DIS [2]. The mean accuracy (mAcc) and mean IoU (mIoU) are reported. Params. represents the trainable parameters.

Methods	Reference	Params. (M)	mAcc (%)	mIoU (%)
Point-MAE [47] (baseline)	ECCV 22	27.02	69.9	60.8
+ Linear probing	-	5.20	63.4	52.5
+ IDPT [88]	ICCV 23	5.64	65.0	53.1
+ Point-PEFT [64]	AAAI 24	5.58	66.5	56.0
+ DAPT [99]	CVPR 24	5.61	67.2	56.2
+ PointGST (ours)	-	5.55	68.4	58.6
ACT [11] (baseline)	ICLR 23	27.02	71.1	61.2
+ Linear probing	-	5.20	64.1	52.0
+ IDPT [88]	ICCV 23	5.64	64.1	52.1
+ Point-PEFT [64]	AAAI 24	5.58	66.0	54.6
+ DAPT [99]	CVPR 24	5.61	64.7	54.5
+ PointGST (ours)	-	5.55	67.6	57.4
RECON [50] (baseline)	ICML 23	27.02	69.7	60.8
+ Linear probing	-	5.20	64.3	51.2
+ IDPT [88]	ICCV 23	5.64	62.9	50.5
+ Point-PEFT [64]	AAAI 24	5.58	65.8	55.8
+ DAPT [99]	CVPR 24	5.61	66.3	56.3
+ PointGST (ours)	-	5.55	67.8	57.9

trainable parameters are noticeably larger than NLP and 2D counterparts and can not generalized well in different point cloud datasets or pre-trained models (see Sec. 6.1.1). In contrast, the proposed PointGST outperforms all other methods with an accuracy of 85.29%, surpassing both IDPT and DAPT, with only 0.6M trainable parameters.

TABLE 8: Comparisons of Parameter-Efficient Fine-Tuning (PEFT) methods from NLP and 2D Vision on the hardest variant of ScanObjectNN [68]. Overall accuracy (%) without voting is reported. Params. represents the trainable parameters.

Method	Reference	Design for	Params. (M)	PB_T50_RS
Point-MAE [40]	ECCV 22	-	22.1	85.18
Linear probing	-	-	0.3	75.99
+ Adapter [23]	ICML 19	NLP	0.9	83.93
+ Perfix tuning [34]	ACL 21	NLP	0.7	77.72
+ BitFit [86]	ACL 21	NLP	0.3	82.62
+ LoRA [24]	ICLR 24	NLP	0.9	81.74
+ DEPT [58]	ICLR 24	NLP	0.3	79.70
+ FourierFT [18]	ICML24	NLP	0.3	78.57
+ VPT-Deep [26]	ECCV 22	2D	0.4	81.09
+ AdaptFormer [7]	NeurIPS 22	2D	0.9	83.45
+ SSF [35]	NeurIPS 22	2D	0.4	82.58
+ FacT [27]	AAAI 23	2D	0.5	78.76
+ BI-AdaptFormer [28]	ICCV 23	2D	0.4	83.66
+ SCT [97]	IJCV 24	2D	0.3	80.40
+ IDPT [88]	ICCV 23	3D	1.7	84.94
+ DAPT [99]	CVPR 24	3D	1.1	85.08
+ PointGST (ours)	-	3D	0.6	85.29

6.6 Visualization Results

Fig. 6 presents the t-SNE [69] feature manifold visualization of models after full fine-tuning, linear probing, and point cloud-customized PEFT methods, IDPT [88] and DAPT [99], alongside our PointGST, applied to the ScanObjectNN PB_T50_RS dataset. Greater dispersion of points among categories indicates better model representation and easier classification. Specifically, as shown in Fig. 6(c-d), the spatial domain tuning-based methods, IDPT and DAPT exhibit greater confusion between categories, while Fig. 6(e) demonstrates that our PointGST enables the pre-trained model to produce more distinguishable representations with fewer learnable parameters in the spectral domain.

6.7 Ablation Study

Following previous methods [88], [99], we conduct ablation studies on the challenging ScanObjectNN PB_T50_RS dataset. Unless otherwise specified, we choose the Point-MAE [47] and PointGPT-L [4] as the baseline, and all experiments are performed without the voting strategy.

6.7.1 The effect of each component

We systematically evaluate the effect of each component within our PointGST by analyzing four key aspects: global spectral, local spectral, residual connections, and spectral inversion. The results are detailed in Tab. 9.

Taking the Point-MAE baseline as an example, without any of our components, the linear probing setting achieves only 75.99% overall accuracy (OA), significantly lower than the fully fine-tuning counterpart by 9.19%. When incorporating either global or local spectral components individually, we observe a marked improvement of 6.00% in OA for both, while introducing only 0.35M additional trainable parameters. Further performance gains are seen when integrating residual connections and applying the inverse Graph Fourier Transform (iGFT) to project back into the spatial domain, aligning with the output of the transformer layer. Ultimately, the combination of all components leads

to a significant increase in accuracy to 85.29% OA. This outcome underscores the complementary nature of global and local spectral representations, which can effectively de-correlate the inner confusion of point tokens and provide task-related intrinsic information to guide the fine-tuning phase.

To further demonstrate the effectiveness of fine-tuning in the spectral domain, we apply different tokens in the proposed Point Cloud Spectral Adapter (Fig. 2(b)), including the default point tokens T_s , initializing a learnable matrix to act on T_s , and our method of transferring the T_s (serving as graph signal) to the spectral tokens. As shown in Fig. 7, the proposed paradigm achieves better performance compared with the other two settings, demonstrating the importance of fine-tuning in the spectral domain.

6.7.2 Ablation study on the hyper-parameters and designs choices of PCSA

The effect of dimension r . The PCSA aims to decrease the trainable parameters during fine-tuning, and the dimension r is chosen to balance efficiency and performance. As shown in Tab. 10a, as the dimension r increases from 12 to 36, the performance of our method improves, with performance increasing from 83.66 to 85.29. However, further increasing r to 96 slightly hurts the performance, with performance dropping to 84.98. Therefore, we set the dimension r to 36 by default, which reports ideal performance and less trainable parameters.

The effect of scale s . The scaling factor s can control the impact of spectral tokens on the task-agnostic tokens. As shown in Tab. 10b, we empirically find that when the value is simply set as 1 without the need for extensive hyper-parameter tuning, the proposed can achieve satisfactory performance.

The effect of different adaption choices. In our PCSA, we utilize a simple shared linear layer to adapt the global and local spectral tokens, shown in Fig. 2(b). Here, we explore other possible learnable choices, including shared Attention, MLP (two layers), DWConv, linear, and individual linear for global and local spectral. Note that for fair comparisons, we make these options meet similar trainable parameters (about 0.6M). The results presented in Tab. 10c validate that the used shared linear layer is simple yet effective compared with other learnable architectures.

6.7.3 The effect of the position of PCSA

We then study the effect of the position of the PCSA. For the inserted layers, we consider the shallow layers and deep layers. Tab. 11a clearly demonstrates that the performance of PointGST has a positive relative to the added layers. Taking the Point-MAE baseline as an example, injecting the PCSA into half of the layers will cause about a 2.12%/1.53% performance drop. Therefore, in our method, we inject the proposed point spectral adapter into all transformer layers. In addition, we also explore the effect of inserted modules. There are three potential choices: FFN, Attention, and each entire transformer block. As shown in Tab. 11b, inserting the PCSA into FFN is able to outperform the Attention and entire transformer block by 1.01% and 1.04% (resp. 0.42%, 0.45%) overall accuracy for Point-MAE (resp. PointGPT-L), respectively.

TABLE 9: The effect of each component of our PointGST. The trainable parameters (Params.) and the overall accuracy (%) on the hardest variant of ScanObjectNN [68] are reported. The results before and after the slash “/” indicate the results when using Point-MAE and PointGPT-L as the baselines, respectively.

Global spectral	Local spectral	Residual	Inverse	Params. (M)	PB_T50_RS
	Full fine-tuning Linear Probing			22.1/360.5 0.27/0.60	85.18/93.40 75.99/91.29
✓	-	-	-	0.62/2.43	81.99/93.88
✓	-	✓	-	0.62/2.43	83.03/94.27
✓	-	-	✓	0.62/2.43	84.07/94.48
✓	-	✓	✓	0.62/2.43	84.52/94.69
-	✓	-	-	0.62/2.43	81.99/94.17
-	✓	✓	-	0.62/2.43	83.38/94.45
-	✓	-	✓	0.62/2.43	83.69/94.55
-	✓	✓	✓	0.62/2.43	83.83/94.62
✓	✓	✓	✓	0.62/2.43	85.29/94.83

TABLE 10: Ablation study on the Point Cloud Spectral Adapter (PCSA), including dimension r , scale s , and the effect of different adaption choices. The trainable parameters (Params.) and the overall accuracy (%) on the hardest variant of ScanObjectNN [68] are reported. The results before and after the slash “/” indicate the results when using Point-MAE and PointGPT-L as the baselines, respectively.

(a) The effect of r .			(b) The effect of scale s .		(c) The effect of different adaption choices.		
Dimension r	Params. (M)	PB_T50_RS	Scale	PB_T50_RS	Module	Params. (M)	PB_T50_RS
12	0.39/1.22	83.66/94.83	0.01	83.41/94.48	Shared Attention	0.67/2.52	84.07/94.76
24	0.50/1.82	84.59/94.41	0.1	83.34/94.80	Shared MLP	0.67/2.52	83.69/94.41
36	0.62/2.43	85.29/94.83	1.0	85.29/94.83	Shared DwConv	0.61/2.41	85.15/94.55
48	0.75/3.05	84.73/94.41	2.0	83.62/94.41	Shared linear	0.62/2.43	85.29/94.83
72	1.00/4.30	84.28/94.34	5.0	71.03/93.72	Independent linear	0.64/2.46	84.80/94.51
96	1.28/5.58	84.98/94.59	10.0	67.52/93.65			

TABLE 11: The effect of inserted position. The trainable parameters (Params.) and the overall accuracy (%) on the hardest variant of ScanObjectNN [68] are reported. The results before and after the slash “/” indicate the results when using Point-MAE and PointGPT-L as the baselines, respectively.

(a) The effect of inserted layers.			(b) The effect of inserted module.	
Layers	Params. (M)	PB_T50_RS	Position	PB_T50_RS
1→6/1→12	0.45/1.51	83.17/94.69	Attention	84.28/94.41
7→12/13→24	0.45/1.51	83.76/94.07	FFN	85.29/94.83
1→12/1→24	0.62/2.43	85.29/94.83	Entire transformer layer	84.25/94.38

6.7.4 Analysis on the point cloud graph construction

The effect of different weighting schemes. To calculate the edge weight between two points in a graph, we employ a data-dependent scaling strategy. Here, we study various weighting schemes, as detailed in Tab. 12a. The most straightforward weighting scheme, Euclidean distance, yields sub-optimal performance with an overall accuracy of 85.15% and 94.73%. As discussed in Sec. 4.2.1, we contend that the closer two points are, the stronger the weight of their relationship should be. Therefore, we propose a data-dependent scaled distance for edge weight, which outperforms Euclidean distance by 0.14% and 0.10% on the Point-MAE and PointGPT-L baselines. Additionally, we evaluate cosine distance and Gaussian similarity [70] for each pair of key points, finding that our proposed data-dependent scaling strategy yields more stable results.

We also try to generate the weights between point tokens instead of the original point cloud. The results of the last two lines indicate poor performance, accompanying extremely

high training costs (about 4 NVIDIA 3090 days). It is reasonable, as the encoded point tokens from the frozen models are hard to bring the intrinsic information of the downstream point cloud. In contrast, constructing the graph from the original downstream point cloud will provide a compact space that involves task-specific information, which effectively achieves targeted tuning.

The effect of different sorting methods and group number k . When constructing local sub-graphs, we sort and categorize the sampled key points into k groups. This part evaluates the impact of various sorting methods, including random, k -nearest neighbors (KNN), and space-filling curves such as Hilbert order, transposed Hilbert order, Z-order, and transposed Z-order. The results presented in Tab. 12b show that random sorting provides the least favorable results, while methods that preserve spatial locality (e.g., KNN and space-filling curves) considerably enhance the performance metrics. Among them, Trans Z-order sorting stands out as the most effective. KNN exhibits

TABLE 12: Analysis on the point cloud graph.

(a) The effect of different edge weights.			(b) The effect of different sorting methods.		(c) The effect of group number k .	
Source	Method	PB_T50_RS	Sort	PB_T50_RS	k	PB_T50_RS
Original point cloud	Euclidean Distance	85.15/94.73	Random	83.83/94.27	w/o sub-graphs	84.52/94.69
	Cosine Distance	83.97/94.41	KNN	84.59/94.45	2	84.04/94.45
	Gaussian Similarity	83.76/94.73	Hilbert-order	84.00/94.45	4	85.29/94.83
	Scaling Strategy (ours)	85.29/94.83	Trans Hilbert-order	84.59/94.34	8	84.04/94.52
Point token	Gaussian Similarity	68.67/94.48	Z-order	84.90/94.24	16	84.84/94.55
	Scaling Strategy (ours)	71.17/94.66	Trans Z-order	85.29/94.83		

TABLE 13: Analysis on the spectral conversion.

Method	PB_T50_RS
Without Fourier Transform	84.04/93.56
Fast Fourier Transform (FFT)	83.69/94.55
Discrete Cosine Transform (DCT)	84.25/94.25
Graph Fourier Transform (GFT)	85.29/94.83

inferior performance, potentially because it does not yield stable results and sometimes aggregates identical points into different groups. In contrast, space-filling curves maintain a consistent scanning pattern, making it easier for models to learn from the data. Besides, as shown in Tab. 12c, we empirically find that the best performance is achieved when k is set as 4.

6.7.5 Analysis on Different Spectral Conversion

We finally investigate the effect of different spectral conversions, including the Fast Fourier Transform (FFT), Discrete Cosine Transform (DCT), and our used Graph Fourier Transform (GFT). As shown in Tab. 13, the results demonstrate the superiority of the GFT we applied. This can be attributed to the fact that the FFT and DCT are designed for regularly sampled or structured data and assume uniform spacing and regularity in the signals, making them unsuitable for processing non-Euclidean point clouds [25]. In contrast, to accommodate the irregular domain of point clouds, we apply the GFT which is well-suited for such data structures and adapts to specific samples.

7 CONCLUSION

In this paper, we propose a novel parameter-efficient fine-tuning (PEFT) method for point cloud learning called PointGST. Unlike previous spatial domain-tuning point cloud PEFT methods, our PointGST shifts fine-tuning to the spectral domain through the proposed Point Cloud Spectral Adapter (PCSA). This approach effectively mitigates confusion among point tokens from frozen models by using orthogonal components to separate them and incorporates task-specific intrinsic information for targeted tuning. Extensive experiments across various challenging datasets demonstrate that PointGST outperforms the fully fine-tuning setting and SOTA point cloud PEFT methods, building new state-of-the-art results. This makes PointGST a practical solution for resource-efficient model adaptation in point cloud tasks. We hope this work can open new directions for efficient fine-tuning in point cloud tasks.

REFERENCES

- [1] Mohamed Afham, Isuru Dissanayake, Dinithi Dissanayake, Amaya Dharmasiri, Kanchana Thilakarathna, and Ranga Rodrigo. Crosspoint: Self-supervised cross-modal contrastive learning for 3d point cloud understanding. In *Proc. of IEEE Intl. Conf. on Computer Vision and Pattern Recognition*, pages 9902–9912, 2022.
- [2] Iro Armeni, Ozan Sener, Amir R Zamir, Helen Jiang, Ioannis Brilakis, Martin Fischer, and Silvio Savarese. 3d semantic parsing of large-scale indoor spaces. In *Proc. of IEEE Intl. Conf. on Computer Vision and Pattern Recognition*, pages 1534–1543, 2016.
- [3] Angel X Chang, Thomas Funkhouser, Leonidas Guibas, Pat Hanrahan, Qixing Huang, Zimo Li, Silvio Savarese, Manolis Savva, Shuran Song, Hao Su, et al. Shapenet: An information-rich 3d model repository. *arXiv preprint arXiv:1512.03012*, 2015.
- [4] Guangyan Chen, Meiling Wang, Yi Yang, Kai Yu, Li Yuan, and Yufeng Yue. Pointgpt: Auto-regressively generative pre-training from point clouds. In *Proc. of Advances in Neural Information Processing Systems*, volume 36, 2024.
- [5] Ling Chen, Gang Wei, and Zhicheng Wang. Pointagcn: Adaptive spectral graph cnn for point cloud feature learning. In *Proc. of Intl. Conf. on Security, Pattern Analysis, and Cybernetics*, pages 401–406. IEEE, 2018.
- [6] Runnan Chen, Youquan Liu, Lingdong Kong, Xinge Zhu, Yuxin Ma, Yikang Li, Yuenan Hou, Yu Qiao, and Wenping Wang. Clip2scene: Towards label-efficient 3d scene understanding by clip. In *Proc. of IEEE Intl. Conf. on Computer Vision and Pattern Recognition*, pages 7020–7030, 2023.
- [7] Shoufa Chen, Chongjian Ge, Zhan Tong, Jiangliu Wang, Yibing Song, Jue Wang, and Ping Luo. Adaptformer: Adapting vision transformers for scalable visual recognition. In *Proc. of Advances in Neural Information Processing Systems*, volume 35, pages 16664–16678, 2022.
- [8] Fan RK Chung. *Spectral graph theory*, volume 92. American Mathematical Soc., 1997.
- [9] Jacob Devlin, Ming-Wei Chang, Kenton Lee, and Kristina Toutanova. Bert: Pre-training of deep bidirectional transformers for language understanding. In *Proc. Annual Meeting of the Association for Computational Linguistics*, pages 4171–4186, 2019.
- [10] Ning Ding, Yujia Qin, Guang Yang, Fuchao Wei, Zonghan Yang, Yusheng Su, Shengding Hu, Yulin Chen, Chi-Min Chan, Weize Chen, et al. Parameter-efficient fine-tuning of large-scale pre-trained language models. *Nature Machine Intelligence*, 5(3):220–235, 2023.
- [11] Runpei Dong, Zekun Qi, Linfeng Zhang, Junbo Zhang, Jianjian Sun, Zheng Ge, Li Yi, and Kaisheng Ma. Autoencoders as cross-modal teachers: Can pretrained 2d image transformers help 3d representation learning? In *Proc. of Intl. Conf. on Learning Representations*, 2023.
- [12] Hilmi E Egilmez, Eduardo Pavez, and Antonio Ortega. Graph learning from data under laplacian and structural constraints. *IEEE Journal of Selected Topics in Signal Processing*, 11(6):825–841, 2017.
- [13] Lue Fan, Yuxue Yang, Feng Wang, Naiyan Wang, and Zhaoxiang Zhang. Super sparse 3d object detection. *IEEE Transactions on Pattern Analysis and Machine Intelligence*, 45(10):12490–12505, 2023.
- [14] Ben Fei, Liwen Liu, Weidong Yang, Zhijun Li, Wen-Ming Chen, and Lipeng Ma. Parameter efficient point cloud prompt tuning for unified point cloud understanding. *IEEE Transactions on Intelligent Vehicles*, 2024.
- [15] Jiajun Fei and Zhidong Deng. Fine-tuning point cloud transformers with dynamic aggregation. In *Proc. of the IEEE Int. Conf. on Robotics and Automation*, pages 9455–9462. IEEE, 2024.
- [16] Tuo Feng, Wenguan Wang, Ruijie Quan, and Yi Yang. Shape2scene: 3d scene representation learning through pre-training on shape data. In *Proc. of European Conference on Computer Vision*, 2024.

- [17] Xiang Gao, Wei Hu, and Guo-Jun Qi. Graphter: Unsupervised learning of graph transformation equivariant representations via auto-encoding node-wise transformations. In *Proc. of IEEE Intl. Conf. on Computer Vision and Pattern Recognition*, pages 7163–7172, 2020.
- [18] Ziqi Gao, Qichao Wang, Aochuan Chen, Zijing Liu, Bingzhe Wu, Liang Chen, and Jia Li. Parameter-efficient fine-tuning with discrete fourier transform. In *Proc. of Intl. Conf. on Machine Learning*, 2024.
- [19] Meng-Hao Guo, Jun-Xiong Cai, Zheng-Ning Liu, Tai-Jiang Mu, Ralph R Martin, and Shi-Min Hu. Pct: Point cloud transformer. *Computational Visual Media*, 7:187–199, 2021.
- [20] Abdullah Hamdi, Silvio Giancola, and Bernard Ghanem. Mvtn: Multi-view transformation network for 3d shape recognition. In *Proc. of IEEE Intl. Conf. on Computer Vision*, pages 1–11, 2021.
- [21] Kaiming He, Xinlei Chen, Saining Xie, Yanghao Li, Piotr Dollár, and Ross Girshick. Masked autoencoders are scalable vision learners. In *Proc. of IEEE Intl. Conf. on Computer Vision and Pattern Recognition*, pages 16000–16009, 2022.
- [22] Cheng-Yao Hong, Yu-Ying Chou, and Tyng-Luh Liu. Attention discriminant sampling for point clouds. In *Proc. of IEEE Intl. Conf. on Computer Vision*, pages 14429–14440, 2023.
- [23] Neil Houlsby, Andrei Giurgiu, Stanislaw Jastrzebski, Bruna Morone, Quentin De Laroussilhe, Andrea Gesmundo, Mona Attariyan, and Sylvain Gelly. Parameter-efficient transfer learning for nlp. In *Proc. of Intl. Conf. on Machine Learning*, pages 2790–2799. PMLR, 2019.
- [24] Edward J Hu, Phillip Wallis, Zeyuan Allen-Zhu, Yuanzhi Li, Shean Wang, Lu Wang, Weizhu Chen, et al. Lora: Low-rank adaptation of large language models. In *Proc. of Intl. Conf. on Learning Representations*, 2021.
- [25] Wei Hu, Jiahao Pang, Xianming Liu, Dong Tian, Chia-Wen Lin, and Anthony Vetro. Graph signal processing for geometric data and beyond: Theory and applications. *IEEE Transactions on Multimedia*, 24:3961–3977, 2021.
- [26] Menglin Jia, Luming Tang, Bor-Chun Chen, Claire Cardie, Serge Belongie, Bharath Hariharan, and Ser-Nam Lim. Visual prompt tuning. In *Proc. of European Conference on Computer Vision*, pages 709–727. Springer, 2022.
- [27] Shibo Jie and Zhi-Hong Deng. Fact: Factor-tuning for lightweight adaptation on vision transformer. In *Proc. of the AAAI Conf. on Artificial Intelligence*, volume 37, pages 1060–1068, 2023.
- [28] Shibo Jie, Haoqing Wang, and Zhi-Hong Deng. Revisiting the parameter efficiency of adapters from the perspective of precision redundancy. In *Proc. of IEEE Intl. Conf. on Computer Vision*, pages 17217–17226, 2023.
- [29] Brian Lester, Rami Al-Rfou, and Noah Constant. The power of scale for parameter-efficient prompt tuning. In *Proc. Conference on Empirical Methods in Natural Language Processing*. Association for Computational Linguistics, 2021.
- [30] Guohao Li, Matthias Muller, Ali Thabet, and Bernard Ghanem. Deepgcn: Can gcn go as deep as cnns? In *Proc. of IEEE Intl. Conf. on Computer Vision*, pages 9267–9276, 2019.
- [31] Jinyu Li, Chenxu Luo, and Xiaodong Yang. Pillarnet: Rethinking network designs for 3d object detection in lidar point clouds. In *Proc. of IEEE Intl. Conf. on Computer Vision and Pattern Recognition*, pages 17567–17576, 2023.
- [32] Mengke Li, Da Li, Guoqing Yang, Yiu-ming Cheung, and Hui Huang. Adapt pointformer: 3d point cloud analysis via adapting 2d visual transformers. *Proc. of European Conference on Artificial Intelligence*, 2024.
- [33] Minglei Li, Peng Ye, Yongqi Huang, Lin Zhang, Tao Chen, Tong He, Jiayuan Fan, and Wanli Ouyang. Adapter-x: A novel general parameter-efficient fine-tuning framework for vision. *arXiv preprint arXiv:2406.03051*, 2024.
- [34] Xiang Lisa Li and Percy Liang. Prefix-tuning: Optimizing continuous prompts for generation. In *Proc. Annual Meeting of the Association for Computational Linguistics*, pages 4582–4597, 2021.
- [35] Dongze Lian, Daquan Zhou, Jiashi Feng, and Xinchao Wang. Scaling & shifting your features: A new baseline for efficient model tuning. In *Proc. of Advances in Neural Information Processing Systems*, volume 35, pages 109–123, 2022.
- [36] Dingkan Liang, Xin Zhou, Wei Xu, Xingkui Zhu, Zhikang Zou, Xiaoqing Ye, Xiao Tan, and Xiang Bai. Pointmamba: A simple state space model for point cloud analysis. In *Proc. of Advances in Neural Information Processing Systems*, 2024.
- [37] Haojia Lin, Xiawu Zheng, Lijiang Li, Fei Chao, Shanshan Wang, Yan Wang, Yonghong Tian, and Rongrong Ji. Meta architecture for point cloud analysis. In *Proc. of IEEE Intl. Conf. on Computer Vision and Pattern Recognition*, pages 17682–17691, 2023.
- [38] Zhi-Hao Lin, Sheng-Yu Huang, and Yu-Chiang Frank Wang. Learning of 3d graph convolution networks for point cloud analysis. *IEEE Transactions on Pattern Analysis and Machine Intelligence*, 44(8):4212–4224, 2021.
- [39] Daizong Liu, Wei Hu, and Xin Li. Point cloud attacks in graph spectral domain: When 3d geometry meets graph signal processing. *IEEE Transactions on Pattern Analysis and Machine Intelligence*, 2023.
- [40] Haotian Liu, Mu Cai, and Yong Jae Lee. Masked discrimination for self-supervised learning on point clouds. In *Proc. of European Conference on Computer Vision*, pages 657–675. Springer, 2022.
- [41] Ilya Loshchilov and Frank Hutter. Decoupled weight decay regularization. In *Proc. of Intl. Conf. on Learning Representations*, 2017.
- [42] Ilya Loshchilov and Frank Hutter. Sgdr: Stochastic gradient descent with warm restarts. In *Proc. of Intl. Conf. on Learning Representations*, 2017.
- [43] Qiang Lu, Chao Chen, Wenjun Xie, and Yuetong Luo. Pointgcn: Deep convolutional networks on 3d point clouds with neighborhood graph filters. *Computers & Graphics*, 86:42–51, 2020.
- [44] Xu Ma, Can Qin, Haoxuan You, Haoxi Ran, and Yun Fu. Rethinking network design and local geometry in point cloud: A simple residual mlp framework. *Proc. of Intl. Conf. on Learning Representations*, 2022.
- [45] Luke Melas-Kyriazi, Christian Rupprecht, and Andrea Vedaldi. Pc2: Projection-conditioned point cloud diffusion for single-image 3d reconstruction. In *Proc. of IEEE Intl. Conf. on Computer Vision and Pattern Recognition*, pages 12923–12932, 2023.
- [46] Guy M Morton. A computer oriented geodetic data base and a new technique in file sequencing. 1966.
- [47] Yatian Pang, Wenxiao Wang, Francis EH Tay, Wei Liu, Yonghong Tian, and Li Yuan. Masked autoencoders for point cloud self-supervised learning. In *Proc. of European Conference on Computer Vision*, pages 604–621. Springer, 2022.
- [48] Charles R Qi, Hao Su, Kaichun Mo, and Leonidas J Guibas. Pointnet: Deep learning on point sets for 3d classification and segmentation. In *Proc. of IEEE Intl. Conf. on Computer Vision and Pattern Recognition*, pages 652–660, 2017.
- [49] Charles Ruizhongtai Qi, Li Yi, Hao Su, and Leonidas J Guibas. Pointnet++: Deep hierarchical feature learning on point sets in a metric space. In *Proc. of Advances in Neural Information Processing Systems*, volume 30, 2017.
- [50] Zekun Qi, Runpei Dong, Guofan Fan, Zheng Ge, Xiangyu Zhang, Kaisheng Ma, and Li Yi. Contrast with reconstruct: Contrastive 3d representation learning guided by generative pretraining. In *Proc. of Intl. Conf. on Machine Learning*, pages 28223–28243. PMLR, 2023.
- [51] Zekun Qi, Runpei Dong, Shaochen Zhang, Haoran Geng, Chunrui Han, Zheng Ge, Li Yi, and Kaisheng Ma. Shapellm: Universal 3d object understanding for embodied interaction. In *Proc. of European Conference on Computer Vision*, 2024.
- [52] Guocheng Qian, Yuchen Li, Houwen Peng, Jinjie Mai, Hasan Hammoud, Mohamed Elhoseiny, and Bernard Ghanem. Pointnext: Revisiting pointnet++ with improved training and scaling strategies. In *Proc. of Advances in Neural Information Processing Systems*, volume 35, pages 23192–23204, 2022.
- [53] Prajit Ramachandran, Barret Zoph, and Quoc V Le. Searching for activation functions. *arXiv preprint arXiv:1710.05941*, 2017.
- [54] Sameera Ramasinghe, Salman Khan, Nick Barnes, and Stephen Gould. Spectral-gans for high-resolution 3d point-cloud generation. In *Proc. of the IEEE Int. Conf. on Intelligent Robots and Systems*, pages 8169–8176. IEEE, 2020.
- [55] Haoxi Ran, Jun Liu, and Chengjie Wang. Surface representation for point clouds. In *Proc. of IEEE Intl. Conf. on Computer Vision and Pattern Recognition*, pages 18942–18952, 2022.
- [56] Yongming Rao, Jiwen Lu, and Jie Zhou. Global-local bidirectional reasoning for unsupervised representation learning of 3d point clouds. In *Proc. of IEEE Intl. Conf. on Computer Vision and Pattern Recognition*, pages 5376–5385, 2020.
- [57] Havard Rue and Leonhard Held. *Gaussian Markov random fields: theory and applications*. Chapman and Hall/CRC, 2005.
- [58] Zhengxiang Shi and Aldo Lipani. Dept: Decomposed prompt tuning for parameter-efficient fine-tuning. In *Proc. of Intl. Conf. on Learning Representations*, 2024.
- [59] David I Shuman, Sunil K Narang, Pascal Frossard, Antonio Ortega, and Pierre Vandergheynst. The emerging field of signal processing on graphs: Extending high-dimensional data analysis to networks and other irregular domains. *IEEE signal processing magazine*, 30(3):83–98, 2013.
- [60] Hongyu Sun, Yongcai Wang, Wang Chen, Haoran Deng, and Deying Li. Parameter-efficient prompt learning for 3d point cloud

- understanding. In *Proc. of the IEEE Int. Conf. on Robotics and Automation*, 2024.
- [61] Shuofeng Sun, Yongming Rao, Jiwen Lu, and Haibin Yan. X-3d: Explicit 3d structure modeling for point cloud recognition. In *Proc. of IEEE Intl. Conf. on Computer Vision and Pattern Recognition*, pages 5074–5083, 2024.
- [62] Yi-Lin Sung, Jaemin Cho, and Mohit Bansal. Lst: Ladder side-tuning for parameter and memory efficient transfer learning. In *Proc. of Advances in Neural Information Processing Systems*, volume 35, pages 12991–13005, 2022.
- [63] Yiwen Tang, Jiaming Liu, Dong Wang, Zhigang Wang, Shanghang Zhang, Bin Zhao, and Xuelong Li. Any2point: Empowering any-modality large models for efficient 3d understanding. *Proc. of European Conference on Computer Vision*, 2024.
- [64] Yiwen Tang, Ray Zhang, Zoey Guo, Xianzheng Ma, Bin Zhao, Zhigang Wang, Dong Wang, and Xuelong Li. Point-peft: Parameter-efficient fine-tuning for 3d pre-trained models. In *Proc. of the AAAI Conf. on Artificial Intelligence*, volume 38, pages 5171–5179, 2024.
- [65] Lyne Tchapmi, Christopher Choy, Iro Armeni, JunYoung Gwak, and Silvio Savarese. Segcloud: Semantic segmentation of 3d point clouds. In *Proc. of Intl. Conf. on 3D Vision*, pages 537–547. IEEE, 2017.
- [66] Gusi Te, Wei Hu, Amin Zheng, and Zongming Guo. Rgcnn: Regularized graph cnn for point cloud segmentation. In *Proc. of ACM Multimedia*, pages 746–754, 2018.
- [67] Cheng-Hao Tu, Zheda Mai, and Wei-Lun Chao. Visual query tuning: Towards effective usage of intermediate representations for parameter and memory efficient transfer learning. In *Proc. of IEEE Intl. Conf. on Computer Vision and Pattern Recognition*, pages 7725–7735, 2023.
- [68] Mikaela Angelina Uy, Quang-Hieu Pham, Binh-Son Hua, Thanh Nguyen, and Sai-Kit Yeung. Revisiting point cloud classification: A new benchmark dataset and classification model on real-world data. In *Proc. of IEEE Intl. Conf. on Computer Vision*, pages 1588–1597, 2019.
- [69] Laurens Van der Maaten and Geoffrey Hinton. Visualizing data using t-sne. *Journal of machine learning research*, 9(11), 2008.
- [70] Ulrike Von Luxburg. A tutorial on spectral clustering. *Statistics and computing*, 17:395–416, 2007.
- [71] Chu Wang, Babak Samari, and Kaleem Siddiqi. Local spectral graph convolution for point set feature learning. In *Proc. of European Conference on Computer Vision*, pages 52–66, 2018.
- [72] Changshuo Wang, Meiqing Wu, Siwei-Kei Lam, Xin Ning, Shangshu Yu, Ruiping Wang, Weijun Li, and Thambipillai Srikanthan. Gpsformer: A global perception and local structure fitting-based transformer for point cloud understanding. In *Proc. of European Conference on Computer Vision*, 2024.
- [73] Hanchen Wang, Qi Liu, Xiangyu Yue, Joan Lasenby, and Matt J Kusner. Unsupervised point cloud pre-training via occlusion completion. In *Proc. of IEEE Intl. Conf. on Computer Vision*, pages 9782–9792, 2021.
- [74] Yue Wang, Yongbin Sun, Ziwei Liu, Sanjay E Sarma, Michael M Bronstein, and Justin M Solomon. Dynamic graph cnn for learning on point clouds. *ACM Transactions ON Graphics*, 38(5):1–12, 2019.
- [75] Ziyi Wang, Yongming Rao, Xumin Yu, Jie Zhou, and Jiwen Lu. Point-to-pixel prompting for point cloud analysis with pre-trained image models. *IEEE Transactions on Pattern Analysis and Machine Intelligence*, 2024.
- [76] Cheng Wen, Jianzhi Long, Baosheng Yu, and Dacheng Tao. Point-wavelet: Learning in spectral domain for 3-d point cloud analysis. *IEEE Transactions on Neural Networks and Learning Systems*, 2024.
- [77] Xiaoyang Wu, Li Jiang, Peng-Shuai Wang, Zhijian Liu, Xihui Liu, Yu Qiao, Wanli Ouyang, Tong He, and Hengshuang Zhao. Point transformer v3: Simpler faster stronger. In *Proc. of IEEE Intl. Conf. on Computer Vision and Pattern Recognition*, pages 4840–4851, 2024.
- [78] Xiaoyang Wu, Yixing Lao, Li Jiang, Xihui Liu, and Hengshuang Zhao. Point transformer v2: Grouped vector attention and partition-based pooling. In *Proc. of Advances in Neural Information Processing Systems*, volume 35, pages 33330–33342, 2022.
- [79] Zhirong Wu, Shuran Song, Aditya Khosla, Fisher Yu, Linguang Zhang, Xiaoou Tang, and Jianxiong Xiao. 3d shapenets: A deep representation for volumetric shapes. In *Proc. of IEEE Intl. Conf. on Computer Vision and Pattern Recognition*, pages 1912–1920, 2015.
- [80] Aoran Xiao, Jiaxing Huang, Dayan Guan, Xiaoqin Zhang, Shijian Lu, and Ling Shao. Unsupervised point cloud representation learning with deep neural networks: A survey. *IEEE Transactions on Pattern Analysis and Machine Intelligence*, 45(9):11321–11339, 2023.
- [81] Saining Xie, Jiatao Gu, Demi Guo, Charles R Qi, Leonidas Guibas, and Or Litany. Pointcontrast: Unsupervised pre-training for 3d point cloud understanding. In *Proc. of European Conference on Computer Vision*, pages 574–591. Springer, 2020.
- [82] Runsen Xu, Xiaolong Wang, Tai Wang, Yilun Chen, Jiangmiao Pang, and Dahua Lin. Pointllm: Empowering large language models to understand point clouds. In *Proc. of European Conference on Computer Vision*, 2024.
- [83] Li Yi, Vladimir G Kim, Duygu Ceylan, I-Chao Shen, Mengyan Yan, Hao Su, Cewu Lu, Qixing Huang, Alla Sheffer, and Leonidas Guibas. A scalable active framework for region annotation in 3d shape collections. *ACM Transactions ON Graphics*, 35(6):1–12, 2016.
- [84] Bruce XB Yu, Jianlong Chang, Haixin Wang, Lingbo Liu, Shijie Wang, Zhiyu Wang, Junfan Lin, Lingxi Xie, Haojie Li, Zhouchen Lin, et al. Visual tuning. *ACM Computing Surveys*, 56(12):1–38, 2024.
- [85] Xumin Yu, Lulu Tang, Yongming Rao, Tiejun Huang, Jie Zhou, and Jiwen Lu. Point-bert: Pre-training 3d point cloud transformers with masked point modeling. In *Proc. of IEEE Intl. Conf. on Computer Vision and Pattern Recognition*, pages 19313–19322, 2022.
- [86] Elad Ben Zaken, Yoav Goldberg, and Shauli Ravfogel. Bitfit: Simple parameter-efficient fine-tuning for transformer-based masked language-models. In *Proc. Annual Meeting of the Association for Computational Linguistics*, pages 1–9, 2022.
- [87] Yaohua Zha, Huizhen Ji, Jinmin Li, Rongsheng Li, Tao Dai, Bin Chen, Zhi Wang, and Shu-Tao Xia. Towards compact 3d representations via point feature enhancement masked autoencoders. In *Proc. of the AAAI Conf. on Artificial Intelligence*, volume 38, pages 6962–6970, 2024.
- [88] Yaohua Zha, Jinpeng Wang, Tao Dai, Bin Chen, Zhi Wang, and Shu-Tao Xia. Instance-aware dynamic prompt tuning for pre-trained point cloud models. In *Proc. of IEEE Intl. Conf. on Computer Vision*, pages 14161–14170, 2023.
- [89] Cha Zhang, Dinei Florêncio, and Philip A Chou. Graph signal processing-a probabilistic framework. *Microsoft Res., Redmond, WA, USA, Tech. Rep. MSR-TR-2015-31*, 2015.
- [90] Cha Zhang, Dinei Florencio, and Charles Loop. Point cloud attribute compression with graph transform. In *Proc. of IEEE Intl. Conf. on Image Processing*, pages 2066–2070. IEEE, 2014.
- [91] Qingru Zhang, Minshuo Chen, Alexander Bukharin, Pengcheng He, Yu Cheng, Weizhu Chen, and Tuo Zhao. Adaptive budget allocation for parameter-efficient fine-tuning. In *Proc. of Intl. Conf. on Learning Representations*, 2023.
- [92] Qijian Zhang, Junhui Hou, Yue Qian, Yiming Zeng, Juyong Zhang, and Ying He. Flattening-net: Deep regular 2d representation for 3d point cloud analysis. *IEEE Transactions on Pattern Analysis and Machine Intelligence*, 45(8):9726–9742, 2023.
- [93] Renrui Zhang, Ziyu Guo, Peng Gao, Rongyao Fang, Bin Zhao, Dong Wang, Yu Qiao, and Hongsheng Li. Point-m2ae: multi-scale masked autoencoders for hierarchical point cloud pre-training. In *Proc. of Advances in Neural Information Processing Systems*, volume 35, pages 27061–27074, 2022.
- [94] Renrui Zhang, Liuhui Wang, Yu Qiao, Peng Gao, and Hongsheng Li. Learning 3d representations from 2d pre-trained models via image-to-point masked autoencoders. In *Proc. of IEEE Intl. Conf. on Computer Vision and Pattern Recognition*, pages 21769–21780, 2023.
- [95] Songyang Zhang, Shuguang Cui, and Zhi Ding. Hypergraph spectral analysis and processing in 3d point cloud. *IEEE Transactions on Image Processing*, 30:1193–1206, 2020.
- [96] Hengshuang Zhao, Li Jiang, Jiaya Jia, Philip HS Torr, and Vladlen Koltun. Point transformer. In *Proc. of IEEE Intl. Conf. on Computer Vision*, pages 16259–16268, 2021.
- [97] Henry Hengyuan Zhao, Pichao Wang, Yuyang Zhao, Hao Luo, Fan Wang, and Mike Zheng Shou. Sct: A simple baseline for parameter-efficient fine-tuning via salient channels. *International Journal of Computer Vision*, pages 1–19, 2023.
- [98] Xiao Zheng, Xiaoshui Huang, Guofeng Mei, Yuenan Hou, Zhaoyang Lyu, Bo Dai, Wanli Ouyang, and Yongshun Gong. Point cloud pre-training with diffusion models. In *Proc. of IEEE Intl. Conf. on Computer Vision and Pattern Recognition*, pages 22935–22945, 2024.
- [99] Xin Zhou, Dingkan Liang, Wei Xu, Xingkui Zhu, Yihan Xu, Zhikang Zou, and Xiang Bai. Dynamic adapter meets prompt tuning: Parameter-efficient transfer learning for point cloud analysis. In *Proc. of IEEE Intl. Conf. on Computer Vision and Pattern Recognition*, pages 14707–14717, 2024.